REPORT DOCUMENTATION PAGE

Form Approved
OMB No. 0704-0188

1. AGENCY USE ONLY (Leave blank)	2. REPORT DATE	3. REPORT TYPE AND DATES COVERED
	000124	FINAL

4. TITLE AND SUBTITLE
FINAL PROGRESS REPORT: DYNAMIC FLAPS ELECTRONIC SCAN ANTENNA
(SBIR PHASE II)

5. FUNDING NUMBERS
(C) N00421-97-C-1077

6. AUTHOR(S)
DANIEL G. GONZALEZ, PH.D.

7. PERFORMING ORGANIZATION NAME(S) AND ADDRESS(ES)
MALIBU RESEARCH ASSOCIATES, INC.
26670 AGOURA ROAD
CALABASAS, CA 91302-1974

8. PERFORMING ORGANIZATION REPORT NUMBER
MRA P347-FINAL

9. SPONSORING / MONITORING AGENCY NAME(S) AND ADDRESS(ES)
NAVAL AIR WARFARE CENTER AIRCRAFT DIVISION
47253 WHALEN ROAD, UNIT 588
CONTRACTS DEPT., BLDG. 588, SUITE 2, CODE 2542
PATUXTENT RIVER, MD 20670-1463

10. SPONSORING / MONITORING AGENCY REPORT NUMBER

11. SUPPLEMENTARY NOTES

12a. DISTRIBUTION / AVAILABILITY STATEMENT
DISTRIBUTION STATEMENT A: APPROVED FOR PUBLIC RELEASE;
DISTRIBUTION IS UNLIMITED.

12b. DISTRIBUTION CODE

13. ABSTRACT (Maximum 200 words)

A dynamic FLAPS™ electronic scan antenna was the focus of this research. The novelty of this SBIR resides in the use of plasma as the main component of this dynamic X-Band phased array antenna. The plasma introduces a hysteresis property to the phasing elements thus enabling the elements to be addressed in a row-column configuration; in other words, the system can be configured in a latching configuration. By using stripline technology in conjunction with plasma, a phased-array antenna can be produced at a much lower cost than conventional phased-array antennas. This major cost savings is due to the reduction of required number of drivers (result of the plasma hysteresis property) and the simpler manufacturing process.

During the Phase II of this SBIR, the major elements of the plasma phased-array antenna were resolved and demonstrated. These include:

- The ability of plasma to create an efficient RF wall by de-tuning a passband circuit.
- The ability of plasma to reflect incident RF with a consistent phase shift.
- Predictable phase shifting.
- Near ideal plasma hysteresis signature using proper gas.
- Integration of the plasma circuit in a stripline configuration using hybrids.

14. SUBJECT TERMS
Dynamic FLAPS™ Electronic Scan Antenna, Plasma, Hysteresis, Low-Cost Phased-Array Antenna, Stripline, X-Band

15. NUMBER OF PAGES
65

16. PRICE CODE

17. SECURITY CLASSIFICATION OF REPORT	18. SECURITY CLASSIFICATION OF THIS PAGE	19. SECURITY CLASSIFICATION OF ABSTRACT	20. LIMITATION OF ABSTRACT
UNCLASSIFIED	UNCLASSIFIED	UNCLASSIFIED	SAR

FINAL REPORT
DYNAMIC FLAPS ELECTRONIC SCAN ANTENNA

SBIR PHASE II
MRA P347-Final

24 January 2000

Prepared By:

Malibu Research Associates
26670 Agoura Road
Calabasas, CA 91302-1974

Prepared For:

Commander
Naval Air Warfare Center
Aircraft Division
Bldg. 2187
Patuxtent River, MD 20670-5304

Prepared Under:

SBIR Phase II Program
Contract No. N00421-97-C-1077
CLIN 0002
CDRL Data Items A001 & A002

Malibu Research

26670 Agoura Road
Calabasas, CA 91302–1974
(818) 880-5494 Fax 880-5499

File: \347\347-Final;dep

TABLE OF CONTENTS

TABLE OF FIGURES

This is the final report on the experimentation, design and test of an X-band electronic scan antenna for the U.S. Navy based on a concept using gas-discharge plasma display technology.

1.0 INTRODUCTION

In this final report is presented the progression of the electronic scan antenna research highlighting the key results and stumbling blocks throughout this SBIR phase II period.

The original premise was to use the FLAPS^{TM} technology, a Malibu Research patent product, and merge it to plasma in order to generate a dynamic phased array antenna. The FLAPS^{TM} technology consists of generating a reflective surface from dipoles of various lengths placed over a ground plane in an array configuration. The dipoles reflect incident RF energy with a phase shift that is dependent on the dipole configuration in relation to the RF frequency. By generating the dipoles via plasma, the reflective surface thus becomes a dynamically steerable antenna. The major advantage of such an antenna is the hysteresis property of the plasma. The hysteresis enabled such an array antenna to be addressed in a latching technique thus considerably reducing the driver requirements and its complexity. To use plasma as the RF reflective element, its conductive properties within the proposed environment and plasma conditions must be sufficient.

The Phase I result of this SBIR demonstrated that plasma could be used as beam steering elements within the FLAPS^{TM} technology. However, what Phase I failed to unveil was twofold:

- Excessive plasma absorption when used as a reflective element.
- Low plasma conductivity due to low plasma electron density.

These findings were later identified in the first stage of the Phase II period. When the expected results were not produced further investigation, both theoretical and experimental, revealed the previously mentioned problems. As a result plasma cannot be used as a reflective element in the proposed environment.

Although plasma cannot be the reflective medium, it was discovered that plasma could be used in a slightly different configuration to produce the sought after dynamically steerable latching array antenna. The revised design makes use of the plasma dielectric perturbation as opposed to relying on the conductivity of the plasma. With this revised antenna design concept, the major advantages of the original premise are maintained, and are as follows:

- Concept revolves around plasma.
- Plasma is the active element of the electronic scan antenna.
- The latching property of the antenna array, due to the plasma hysteresis.
- Considerable cost savings over conventional phased array systems.

Following this enlightenment, it was decided to build an in-house chamber in order to speed up the data acquisition as well as to enable full control (over the

"controllable" parameters of plasma) of the plasma properties. This turned out to be the key factor in successfully producing the plasma phase shifter element. Throughout the plasma phased-array antenna research major stumbling blocks were overcome; namely:

- Viability of plasma within a stripline circuit.
- Optimum stripline configuration, including plasma firing mechanism.
- Produce and demonstrate a one-bit plasma phase shifter.
- Generating an environment promoting the plasma hysteresis.

The research progression is presented in the following sections in detail.

2.0 INITITAL RESEARCH OF PHASE II

The premise of this SBIR was to develop a Low-Cost Phased-Array antenna by merging two technologies, the plasma and Malibu Research FLAPS™ (FLAt Parabolic Surface) phased surface technology. Plasma enables a latching addressing scheme, thus reducing the complexity and cost of the drivers. The FLAPS™ technology transforms a flat dipole surface in parabolic reflector. By merging both technologies, the focal point of the flat dipole surface can be dynamically scanned. The results of the SBIR Phase I (Contract #N62269-95-C-0154) demonstrated 60 degree beam-scanning with a discrete plasma-element mini-array antenna. These initial results confirmed the vision of producing a dynamic FLAPS™ electronic scan antenna.

The initial research of Phase II consisted of identifying possible design candidates, building the test sample on glass substrates and conducting preliminary tests.

2.1 PLASMA ELEMENT CANDIDATES

Three plasma element candidates were identified; they consist of the continuous dipole, the quantized dipole and the dipole bits, see **Figure 2.1-1**. The pros and cons of each candidate are presented in **Table 2.1-1**. At the time, the best candidate was the quantized dipole since it would require less plasma and would be easier to bench test.

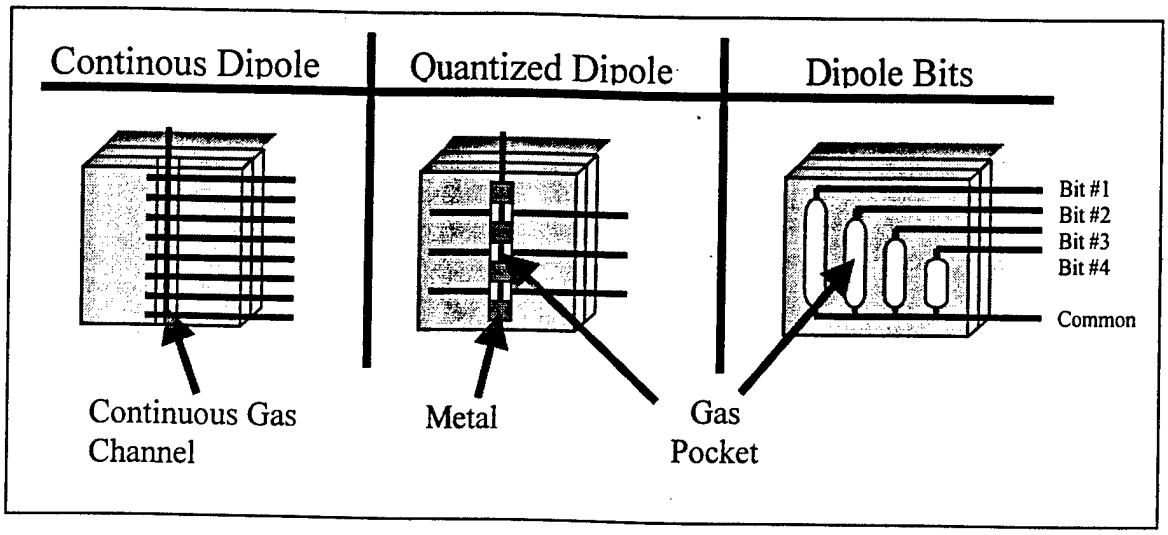

FIGURE 2.1-1 PLASMA ELEMENT CANDIDATES

TABLE 2.1-1 CANDIDATES' PROS & CONS

	Continuous Dipole	Quantized Dipole	Dipole Bits
Pros	▪ Continuous dipole length control ▪ Most adaptable to multi-band operation ▪ Naturally set up for matrix drive	▪ Adaptable lengths ▪ Natural matrix addressing ▪ Less plasma needed ▪ Identifiable development procedure (easier to bench test)	▪ Electrodes all run horizontally (should solve the RF interference problem)
Cons	▪ Pixel connectivity/ uniformity unknown ▪ Maximum electrode interference ▪ Difficult development process	▪ Quantized phase states	▪ May not have high enough electron density (most of tube plasma is in the "positive column" state) ▪ Requires high voltage to excite ▪ Electrode routing issue for a large array

2.2 TESTING CONCEPT

The next step was to define a way to establish the RF properties of the elemental plasma cell. The fact is that the individual cell is too small to radiate at in open space, the results would be corrupted by the apparatus reflections. Thus, the RF test of the elements needs to be performed in an enclosed circuit, i.e. in a stripline configuration. In **Figure 2.2-1** is shown a block diagram of the test setup which consist of an RF generator, a directional coupler, a reference portion with an adjustable phase, a detector and the test sample.

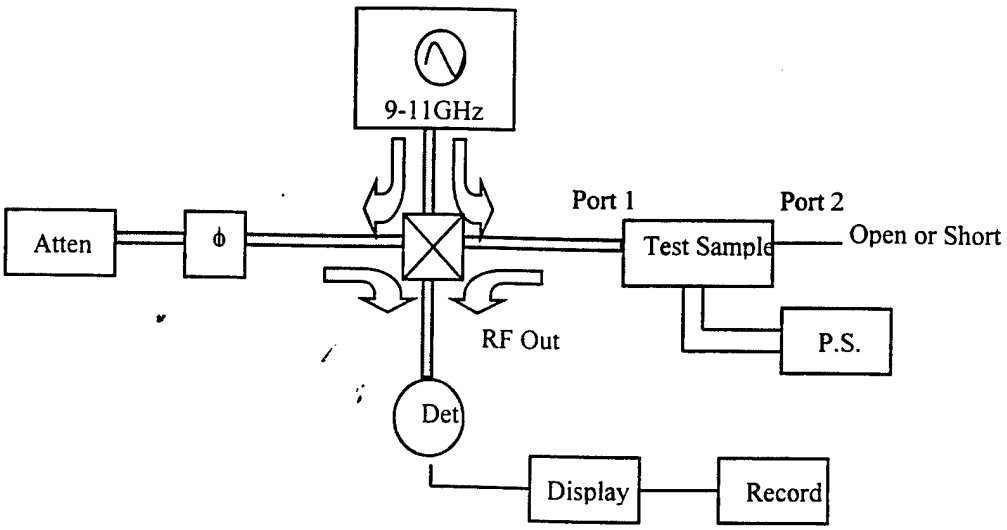

FIGURE 2.2-1 BLOCK DIAGRAM OF TEST SETUP

Two venues are chosen to produce the test samples:

- Contract out to TVI (Technical Vision Inc.) to produce samples on glass substrate.
- Build in parallel at MRA samples using Nixie Tubes.

A diagram of a test sample is shown in **Figure 2.2-2** and pictures of a test sample from TVI, in **Figure 2.2-3**, and using Nixie Tubes, in **Figure 2.2-4**.

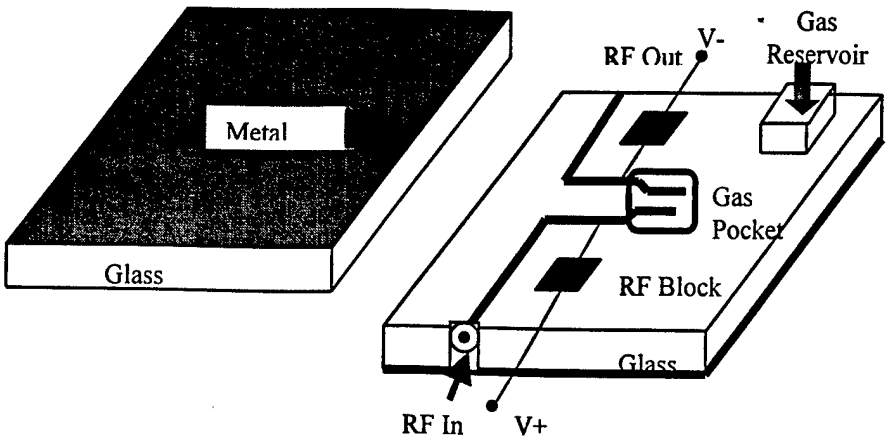

FIGURE 2.2-2 BLOCK DIAGRAM OF TEST SAMPLE

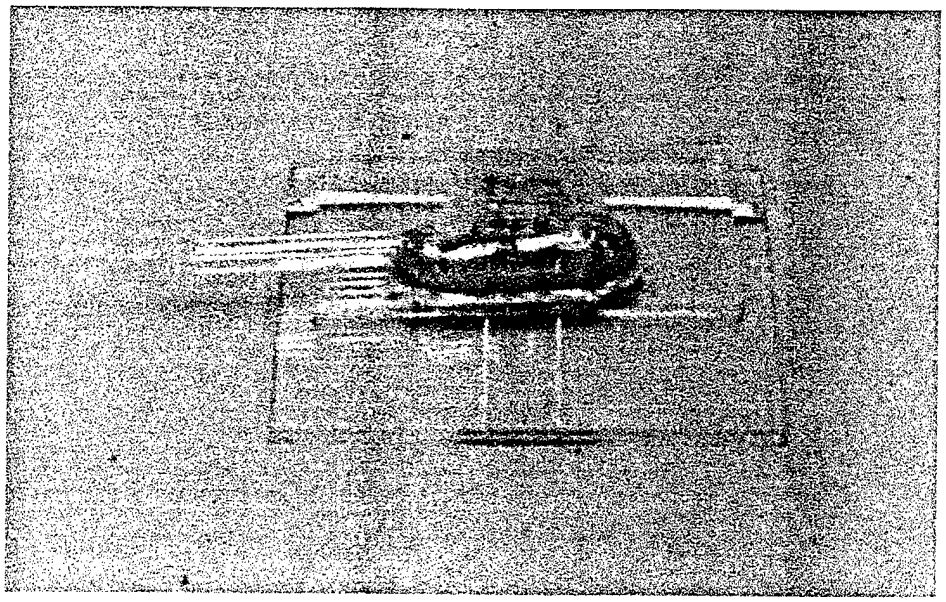

FIGURE 2.2-3 PICTURE OF TEST SAMPLE FROM TVI

2.3 THE PLASMA SWITCH CONCEPT

A stripline configuration including electrodes within a gas pocket is an excellent way of characterizing the plasma. When no plasma is present, the electrodes will act as an RF passband that will be distorted by the presence of plasma. In **Figure 2.3-1** is shown the stripline configuration. The injected RF, at Port 1, travels through the stripline and gets reflected at Port 2 (Port 2 is either short-circuited or open circuited) when no plasma is present. With the presence of plasma, part of the RF energy will be reflected or attenuated at the plasma region and part will be transmitted through. A DC bias voltage

applied to the electrodes via an RF transparent DC path (an RF block) induces plasma. When voltage is applied to the gas immersed electrodes, some gas electrons separate from the atoms creating an ionized region, the plasma.

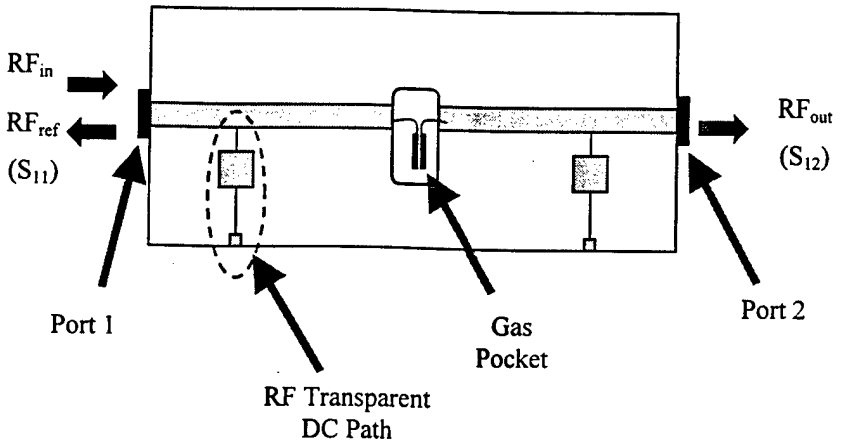

FIGURE 2.3-1 THE STRIPLINE CONFIGURATION

Shown in **Figure 2.3-2** is the equivalent DC circuit (Figure 2.3-2b) of the stripline configuration (Figure 2.3-2a). In Figure 2.3-2 a & b are shown the equivalent DC representation of the electrodes to the DC current between points A & B with and without plasma. Without plasma, no current can flow across the electrodes due to the gap between them; therefore, the electrodes look like an open circuit or a capacitor. Plasma creates a DC path to the current across the electrodes.

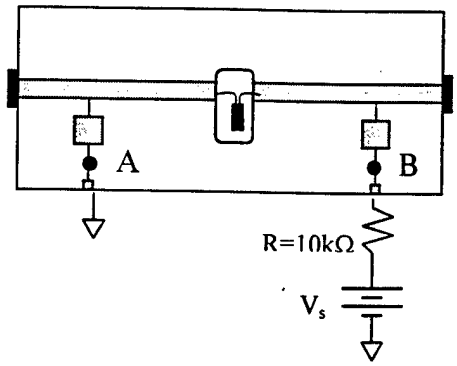

a) Stripline Configuration

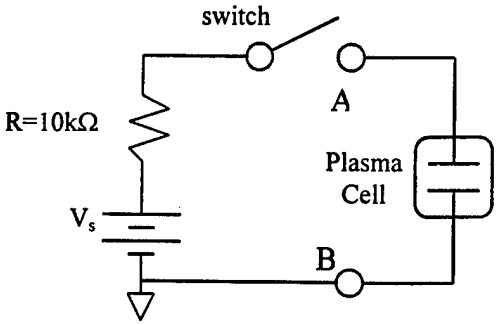

b) DC Equivalent Circuit

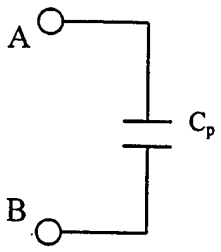

c) Electrode Representation without Plasma

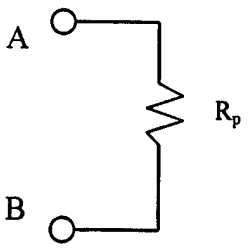

d) Electrode Representation with Plasma

FIGURE 2.3-2 THE STRIPLINE EQUIVALENT DC CIRCUIT

In **Figure 2.3-3** is presented the equivalent RF circuit (Figure 2.3-3b) of the stripline configuration (Figure 2.3-3a). In Figure 2.3-3 a & b are shown the equivalent RF representation of the electrodes to the DC current between points A & B with and without plasma. Without plasma, RF can propagate across the electrodes within the passband of the circuit since the electrodes are tightly coupled. The presence of plasma creates a wall to the incident RF energy and thus reflects or absorbs the energy.

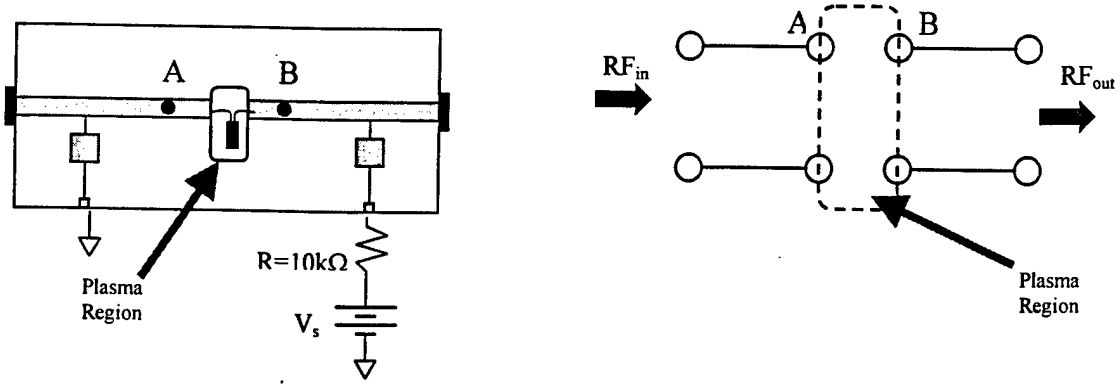

a) Stripline Configuration

b) RF Equivalent Circuit

c) Electrode RF Representation

d) Plasma RF Representation

FIGURE 2.3-3 THE STRIPLINE EQUIVALENT RF CIRCUIT

2.4 PHASE II PRELIMINAY TEST RESULTS

Parallel testing was conducted using the glass substrate samples created by TVI and the Nixie Tube stripline circuits. Within the stripline circuit, the plasma behaves well. The glass substrate sample results are shown in **Figure 2.4-1**. Notice the passband of the circuit between 5.5GHz and 7GHz with a low insertion loss (<2dB). On the same plot is shown the insertion loss (S21, the ratio of the transmitted energy to the incident energy) of the circuit, with the presence of plasma, for various gas pressure. It is seen here that the efficiency of plasma to block the incident RF energy is dependent on the pressure of the gas within the electrode area. On average, the plasma blocks 10dB of the incident RF energy.

In **Figure 2.4-2** results of the Nixie Tube configuration are shown. With the Nixie Tube the passband is centered around 10.1GHz (seen on the 0vts curve). Here the efficiency of plasma to block RF energy is measured as a function of DC applied voltage to the electrodes. In this case the plasma blocks the RF energy by at least 25dB when a DC voltage of 80 is applied to the electrodes.

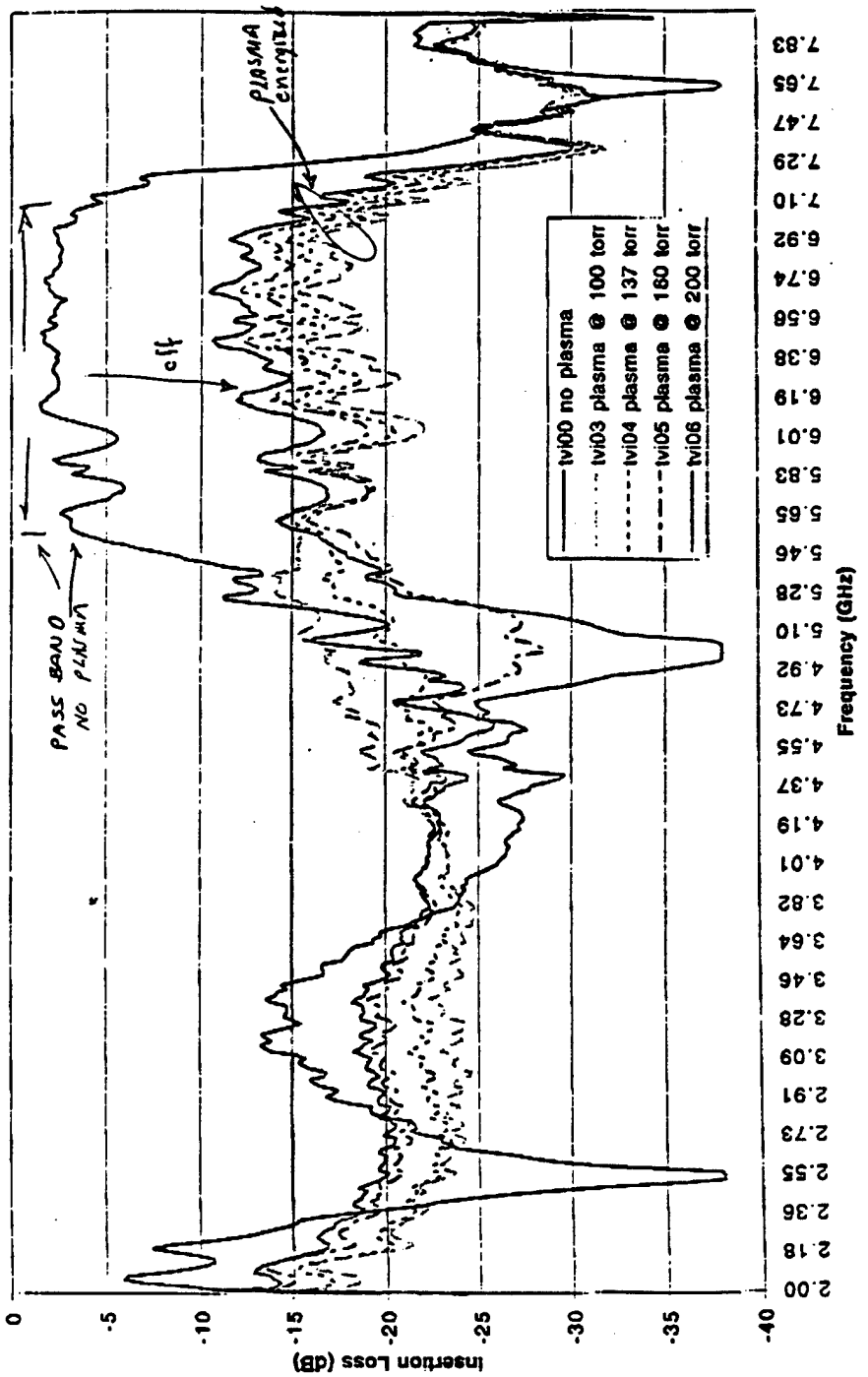

FIGURE 2.4-1 INSERTION LOSS OF GLASS SUBSTRATE AS A FUNCTION OF PRESSURE

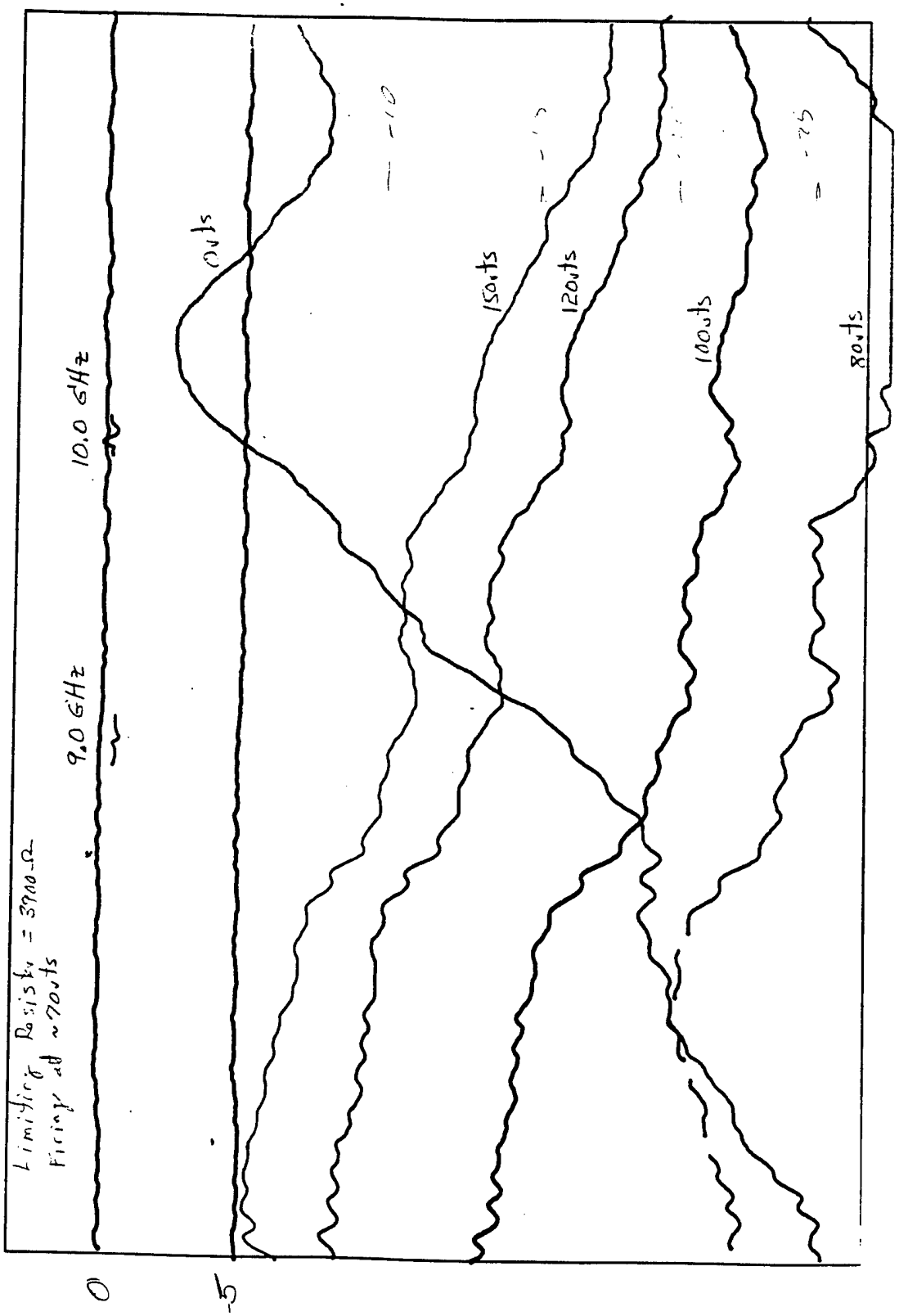

FIGURE 2.4-2 INSERTION LOSS OF NIXIE TUBE SAMPLE AS A FUNCTION OF DC VOLTAGE

2.5 INITIAL OBSERVATIONS

Initial testing demonstrated the efficiency of plasma to block the incident RF energy. Furthermore this testing showed that the Neon-Argon (NeAr) gas mixture was the better choice of all the mixture tested. The turn-around time to produce monolithic glass sample was between 2-3 weeks, which considerably reduced the progress of the research. Acceleration of sample production was necessary, as was having more control over the plasma parameters.

After the success of these preliminary tests, an initial mini-glass substrate array was manufactured and tested. The idea was to observe a beam scan of the glass substrate plasma array antenna. The mini-array was subjected to a plane wave and the reflected wave was to be measured. It turned out that the initial result did not reflect what was anticipated. Most of the energy went through the array; there was minimal reflected energy. It was realized that creating a virtual wire out of plasma seemed to be problematic. The observed plasma phenomenon also demonstrated that it could create a phase shift in the stripline test circuit.

To better understand the plasma phenomenon, Dr Paul Bellan, a plasma physicist from CalTech, was included in the team as a consultant.

3.0 THEORETICAL PLASMA ANALYSIS

Presented in this section is a plasma theoretical analysis focusing on the importance of the collision frequency, electron density and skin-depth to the conductivity of plasma. The original concept of the gas-discharging plasma displays was to use the monochromatic display as the reflecting surface, where dipole elements of modulable length would be created dynamically via the display's plasma pixels. As will be demonstrated, the plasma conductivity is very low therefore the efficiency of using plasma as a dipole is considerably reduced.

3.1 DERIVING THE SKIN DEPTH EQUATIONS

To act as a dipole, the plasma reflecting properties must be in close proximity to a metal conductor. Basically when plasma is present, it has to display high conductivity to the impinging electric fields; in other words, its skin depth must be small compared to the impinging electric field wavelength. There are two kinds of skin depth, the collisional and the collisionless skin depth. In the following, the theory leading to the skin depth is derived.

The derivation starts, as do most electromagnetic derivations, from Maxwell's equation to which are coupled: Ampere's Law, Faraday's Law and Newton's electron force equation.

$$\nabla \times \mathbf{E} = -\frac{\partial \mathbf{B}}{\partial t} \tag{1}$$

$$\nabla \times \mathbf{B} = \mu_0 \mathbf{J} + \varepsilon_0 \mu_0 \frac{\partial \mathbf{E}}{\partial t} \tag{2}$$

$$m_e \frac{d\mathbf{v}}{dt} = q_e \mathbf{E} - v_e m_e \mathbf{v} \tag{3}$$

Where v_e is the collision frequency (also known as the collisional drag) on the electrons due to the collisions with the ions and neutrons , m_e is the electron mass and q_e is the electron charge. In this plasma application, the collisions with neutrons are the main contributors to the collisional drag since the plasma is weakly ionized. In the frequency domain, equation (3) can be re-written as

$$\mathbf{v} = \frac{q_e \mathbf{E}}{-i\omega m_e + v_e m_e} = \frac{q_e \mathbf{E}}{-i\omega m_e (1 + i v_e/\omega)} \tag{4}$$

From equation (4) are defined the collisional and collisionless regions as:

Collisional => $v_e/\omega >> 1$

Collisionless => $v_e/\omega << 1$

Thus in the collisionless regime, the electron velocity is effectively independent of the collision frequency v_e.

Using the definition of both regimes, the skin depth of the plasma can be derived by defining first the propagation constant k via the corresponding wave equation. Along the way the plasma frequency will be defined.

Taking the curl of equation (1) (Faraday's Law) one obtains:

$$\nabla \times \nabla \times \mathbf{E} = -\frac{\partial}{\partial t}(\nabla \times \mathbf{B}) \tag{5}$$

which, after using vector identities and assuming that the wave is transverse, becomes

$$\begin{aligned} \nabla^2 \mathbf{E} &= \mu_0 \frac{\partial \mathbf{J}}{\partial t} + \varepsilon_0 \mu_0 \frac{\partial^2 \mathbf{E}}{\partial t^2} \\ &= -i\omega\mu_0 \mathbf{J} - \omega^2 \mu_0 \varepsilon_0 \mathbf{E} \end{aligned} \tag{6}$$

The current **J**, is mainly propagated by the electrons, and thus is given as

$$\mathbf{J} = n_e q_e \mathbf{v} \tag{7}$$

where n_e is the electron density. Replacing equation (7) into Newton's electron force equation, (4), one can derive the plasma frequency (an important parameter in the plasma world).

$$\begin{aligned} \mathbf{J} &= \frac{n_e q_e^2 \mathbf{E}}{-i\omega m_e (1 + i\nu_e / \omega)} \\ &= \varepsilon_0 \left\{ \frac{n_e q_e^2 \mathbf{E}}{-i\omega m_e \varepsilon_0 (1 + i\nu_e / \omega)} \right\} \end{aligned} \tag{8}$$

from which the plasma frequency is defined as:

$$\omega_{pe}^2 = \frac{n_e q_e^2}{\varepsilon_0 m_e} \tag{9}$$

Substituting equation (9) into (8) and the result in the wave equation, (6), the following is obtained:

$$\nabla^2 \mathbf{E} = \left\{ \frac{\omega_{pe}^2}{(1 + i\nu_e / \omega)} - \omega^2 \right\} \mu_0 \varepsilon_0 \mathbf{E} \tag{10}$$

The solution to the wave equation is then given as

$$\left\{ \frac{\omega_{pe}^2}{(1 + i\nu_e / \omega)} - \omega^2 + k^2 c^2 \right\} \mathbf{E} = 0 \tag{11}$$

where $c^2 = 1/(\varepsilon_0 \mu_0)$, is the speed of light. From (11) is obtained the so-called wave dispersion relation:

$$\omega^2 = \frac{\omega_{pe}^2}{(1 + i\nu_e / \omega)} + k^2 c^2 \tag{12}$$

In this application, the plasma is assumed to have a sufficiently high density such that the left-hand term in the dispersion relation can be ignored.

$$\omega^2 << \frac{\omega_{pe}^2}{(1 + i\nu_e / \omega)}$$

Thus,

$$k^2 = -\frac{\omega_{pe}^2}{(1 + i\nu_e / \omega) \cdot c^2} \tag{13}$$

Note that the smallest k value between both regimes will dominate. Now let's derive the skin depth for both regimes.

3.1.1 The Collisionless Regime

The collisionless regime was defined as

$$v_e/\omega << 1$$

Thus, equation (13) becomes

$$k^2 = -\frac{\omega_{pe}^2}{c^2} \tag{14}$$

Which means that the wave will be evanescent, thus exponentially decaying at a rate of $e^{(-x\omega_{pe}/c)}$. The skin depth is defined as the distance for the electric field to decay by a factor of e^{-1}. Therefore,

$$\partial_{collisionless} = \frac{c}{\omega_{pe}} = \frac{5x10^5}{\sqrt{n}}\text{cm} \tag{15}$$

where n is the density per cm cube. In the collisionless regime the skin depth is independent of the frequency.

3.1.2 The Collisional Regime

The collisional regime is defined as $v_e/\omega >> 1$, thus equation (13) becomes

$$k^2 = -\frac{\omega_{pe}^2 \cdot \omega}{iv_e \cdot c^2} \tag{16}$$
$$= i\frac{\mu_0 \cdot n_e \cdot q_e^2 \omega}{m_e \cdot v_e}$$

In the collisional regime, equation (8) can be expressed in terms of the electrical resistivity as

$$\mathbf{J} = \frac{n_e q_e^2 \mathbf{E}}{v_e \cdot m_e} = \frac{1}{\eta}\mathbf{E} \tag{17}$$

From which equation (15) may be expressed in terms of the electric resistivity, η, as

$$k^2 = -\frac{\omega_{pe}^2 \cdot \omega}{i v_e \cdot c^2} = i\frac{\mu_0 \omega}{\eta} \tag{18}$$

The wave will have an evanescent mode exponentially decaying at the rate defined by the real part in the exponential term solving to the wave equation. The exponential term is:

$$\exp(ikx) = \exp(i\sqrt{i\mu_0\omega/\eta} \cdot x \tag{19}$$

Thus, the collisional skin depth is

$$\partial_{collisional} = \sqrt{\frac{2\eta}{\mu_0 \omega}} \tag{20}$$

3.2 PREDICTING THE PLASMA SKIN DEPTH

As mentioned earlier, the plasma reflecting properties must be fairly close to a metal conductor to act as a dipole. In other words, the skin depth presented by the plasma to the impinging field has to be as close as possible to the skin depth of a metal. To grasp the implication of this statement a comparison between the skin depth of metal, copper, and plasma is presented.

3.2.1 Skin Depth of Copper

The copper's parameters are:

- $n_e = 10^{23}\ \text{cm}^{-3}$
- $\eta = 1.8\text{x}10^{-8}\ \Omega/\text{m}$

Therefore at 9.0GHz the copper's skin depths for both regimes are:

⇒ Collisionless

$$\partial_{collisionless} = \frac{5\times10^{5}}{\sqrt{10^{23}}}cm = 1.6\times10^{-6}\,cm$$

⇒ Collisional

$$\partial_{collisional} = \frac{1.8\times10^{-8}\,\Omega/m}{\sqrt{4\times10^{-6}\pi^{2}\cdot9\times10^{9}}} = 2.25\times10^{-7}\,m = 2.25\times10^{-5}\,cm$$

The effective skin depth of copper is $2.25\text{x}10^{-5}$cm (since it's the largest of both, remember that the dominant regime is the one that "produces" the smallest k which is inversely proportional to the skin depth).

3.2.2 Skin Depth of Plasma

The plasma density will be in the range of $n_e = 10^{12}$ cm^{-3}

$\Rightarrow$ Collisionless

$$\partial_{collisionless} = \frac{5\times10^5}{\sqrt{10^{12}}} cm = 0.5cm$$

Even without calculating the collisional skin depth, it is seen from the plasma collisionless skin depth that the copper's skin depth is in the order of 20,000 times smaller than that of the plasma, see **Table 3.2.2-1**. Therefore, plasma cannot be considered as an equivalent to metal by no means.

It is conclusive that plasma will not act as a dipole. It is not a good passive reflector (plasma does not act as a metal conductor to an impinging field). However, as will be demonstrated in the following section, plasma can be used as a good RF block/reflector within a circuit.

TABLE 3.2.2-1 SKIN DEPTH OF COPPER VS PLASMA @ 9GHZ

	n_e (cm^{-3})	η(Ω/m)	Collisional	Collisionless
Copper	1.0E23	1.8E-8	2.25E-5 cm	1.6E-6 cm
Plasma	1.0E12			0.5 cm

3.3 THEORETICAL ANALYSIS OUTCOME

Theoretical analysis demonstrated that plasma conductivity is very low and thus, renders the initial concept of using plasma as a dynamic dipole non-realistic. Although plasma cannot be used as a pure dipole, in the initial research leg of Phase II it was seen that plasma could be used in a stripline configuration as an RF wall, some sort of a switch with hysteresis.

Following these results, a revised antenna design concept was brought forward. While the design was modified, the major advantages of the original premise were maintained. These are:

- Concept revolves around plasma.
- Plasma is the active element of the plasma phased-array antenna.
- Plasma hysteresis enables a latching configuration.
- Considerable cost savings over conventional phased-array systems.

In order to continue the research at an accelerated pace, an in-house test chamber needed to be built. This would allow us to have full control over the major plasma parameters. Furthermore, new test samples were designed in order to increase throughput.

4.0 IN-HOUSE TEST CHAMBER

As mentioned in the previous section, an in-house vacuum test chamber would reveal itself to be very beneficial. The major reasons for building such a system are as follows:

- The subcontractor's sample turn around was too slow.
- Needed to increase throughput of experiments.
- To have full control over the plasma key parameters.
- Decrease the cost of producing test samples.

In this section is presented the fully assembled test setup including some photos of the arrangement as seen in **Figure 4.0-1**.

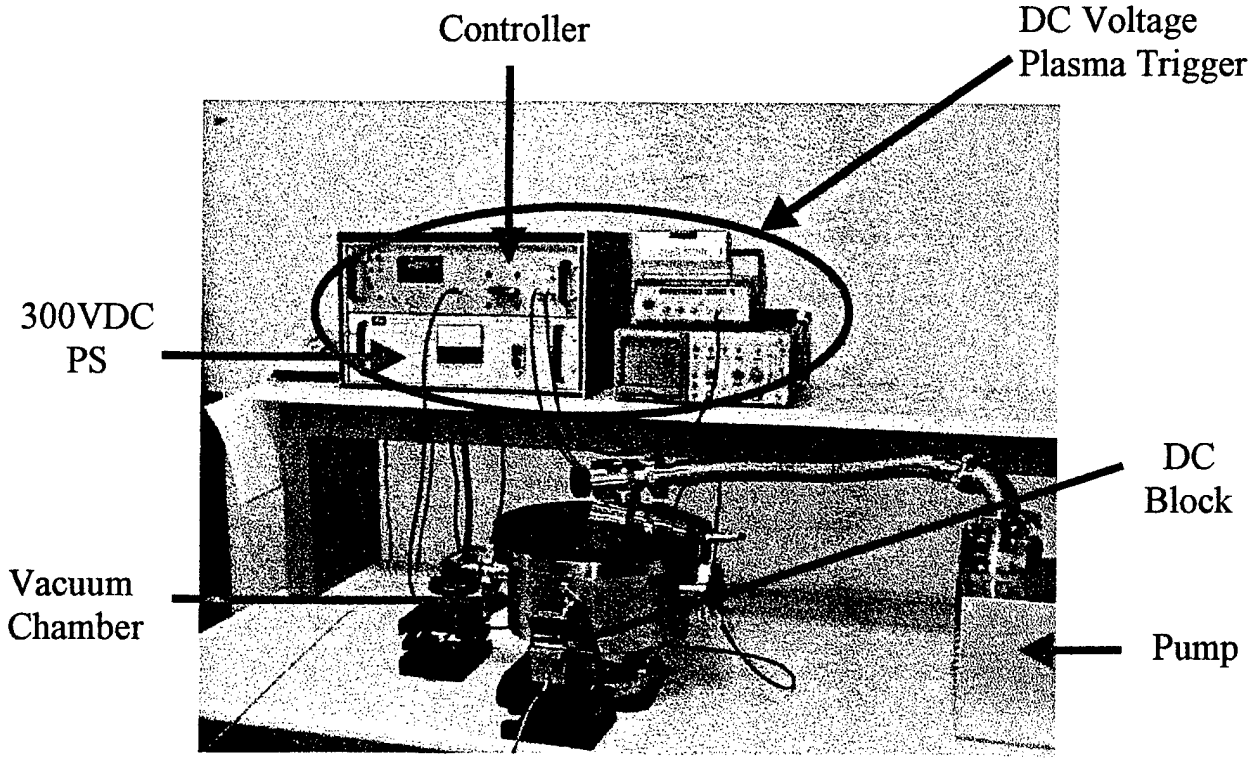

FIGURE 4.0-1 IN-HOUSE VACUUM TEST CHAMBER

In **Figure 4.0-2** is a photo of a stripline test sample in the vacuum chamber with the top portion lifted and the plasma firing between the electrodes.

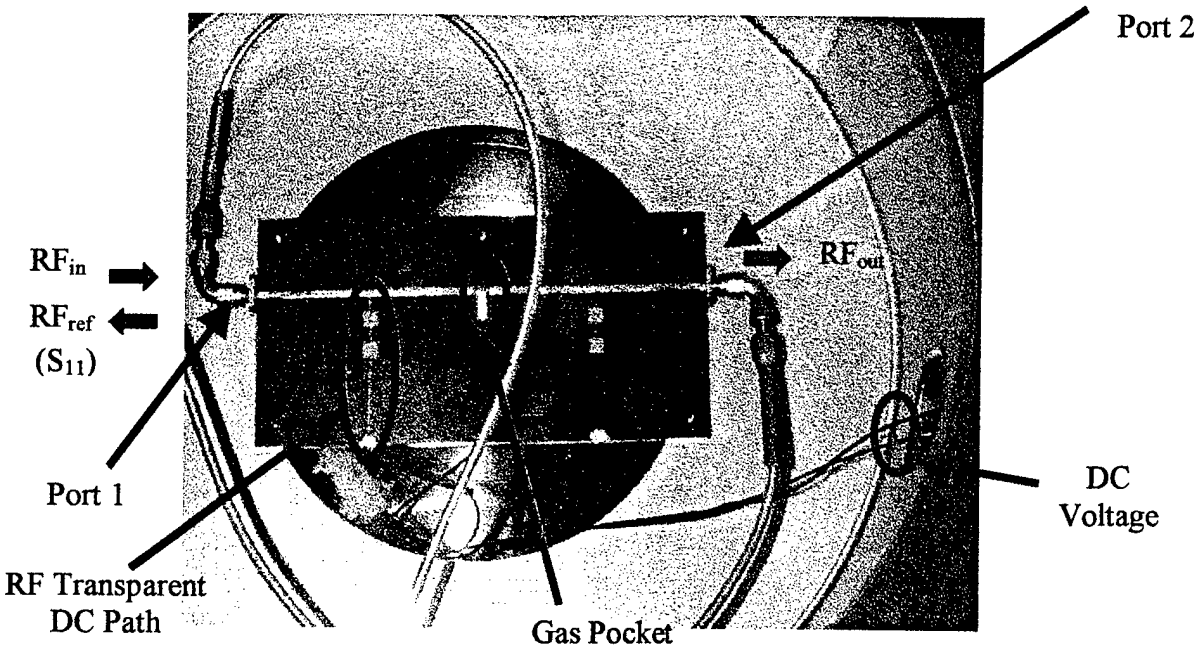

FIGURE 4.0-2 TEST SAMPLE WITH PLASMA FIRED

4.1 THE STRIPLINE TEST SAMPLES

The stripline test samples are conventional stripline technology, copper transmission line etched over a dielectric medium, in which a pocket is machined out and electrodes are introduced. The stripline test samples are inserted into the vacuum chamber in which air is pumped out and replaced by a pure gas. The stripline is a simple 50Ω transmission line surrounded by a duroid medium ($\varepsilon_r = 2.2$) and slotted in the middle where an air gap is machined. To each end of the transmission line are then soldered electrodes extending well into the air gap. The DC plasma triggering/sustaining voltage is applied to the electrodes via four quarter-wavelength impedance mismatch between the

DC power supply and the transmission lines, two per transmission line. The impedance mismatch renders the DC path invisible to the RF within the stripline. A typical stripline test sample described above is shown in **Figure 4.0-2** with the top portion lifted and the plasma firing between the electrodes.

The plasma is characterized by taking insertion loss measurements of the stripline with and without its presence while varying the sensitive parameters. **Figure 4.1-1** shows how the insertion loss is measured (P_{in} & P_{out} are the input and output power respectively).

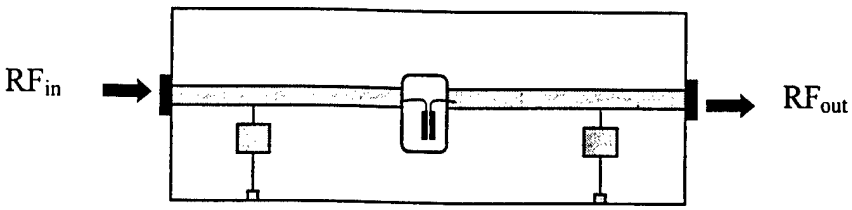

$IL = 10 \log (P_{out}/P_{in})$
$IL = 0$ dB ; for $P_{out} = P_{in}$
$= -3$ dB ; for $P_{out} = P_{in}/2$
$IL_{ideal} \geq -20$dB in presence of plasma

FIGURE 4.1-1 INSERTION LOSS OF THE TEST SAMPLE

4.2 INITIAL CHARACTERIZATION OF THE PLASMA

The result of having an in-house vacuum test chamber was to substantially increase the throughput of the measurements. It was easier and faster to change the sensitive variables on-the-fly. These parameters include the gas pressure; DC applied voltage and current limiting resistor. With one test sample a slew of data was now possible due to the availability of such a test chamber. In **Figure 4.2-1 a-c** is shown the

insertion loss of a test sample under full investigation. One parameter is held constant while the other two are scanned. Looking at Figure 4.2-1c one notices the so-called "sweet spot" near 30 Torrs with maximum insertion loss with the case of a current limiting resistor of 11kΩ. These results enabled a better understanding of the RF interaction with plasma.

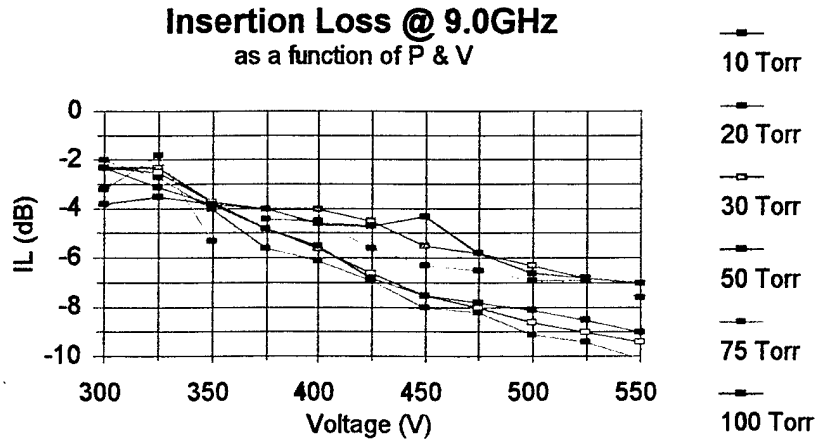

FIGURE 4.2-1A SAMPLE INSERTION LOSS AS A FUNCTION OF PRESSURE & VOLTAGE

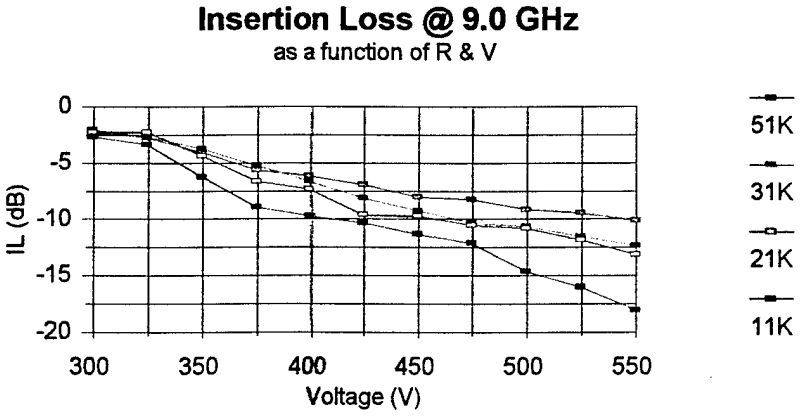

FIGURE 4.2-1B SAMPLE INSERTION LOSS AS A FUNCTION OF VOLTAGE & RESISTOR

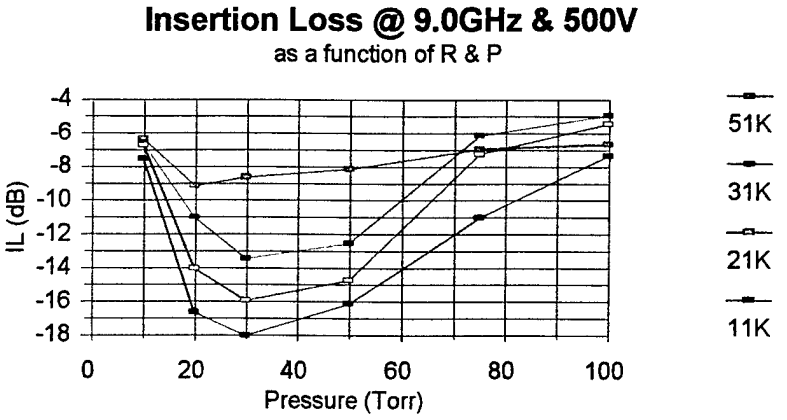

FIGURE 4.2-1C SAMPLE INSERTION LOSS AS A FUNCTION OF RESISTOR & PRESSURE

4.3 TEST CONFIGURATION SAMPLES

A slew of test samples was generated in order to determine the most efficient stripline design. Efficient in the following sense:

- define the optimum firing method (that which yields the highest RF insertion loss);
- determine the simpler manufacturing method yielding adequate RF insertion loss.

The major configurations tested were:

- Electrode-to-electrode

  Consists of inserting a gap in the middle portion of the stripline and coupling the RF energy from one side of the stripline to the other via two electrodes soldered on each end of the stripline, see **Figure 4.3-1a.**

- Electrode-to-stripline

  An electrode is inserted between the stripline and the ground plane in order to disrupt the RF energy, shown in **Figure 4.3-1b.**

- Stripline-to-ground

  Consists of soldering a piece of copper to the stripline, see **Figure 4.3-1c.**

- Stripline-to-stripline

  In terms of manufacturing cost, this configuration would be the least expensive. The coupling transmission lines are printed on each of the stripline plates and inserted between the plates is a thin dielectric plate with gas pocket where the stripline couples, see **Figure 4.3-1d.**

Out of the different samples tested the electrode-to-electrode configuration yielded the best results. Previously, only the insertion loss was measured. As a result we had to ask, Is the plasma acting as an RF wall or an RF absorber?

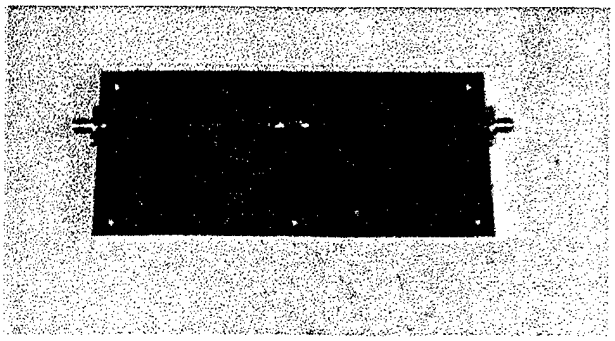

A) Electrode-to-Electrode

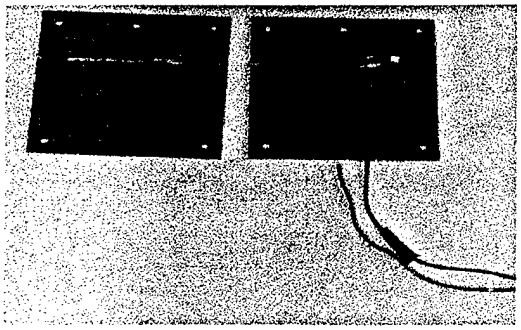

B) Electrode-to-Stripline

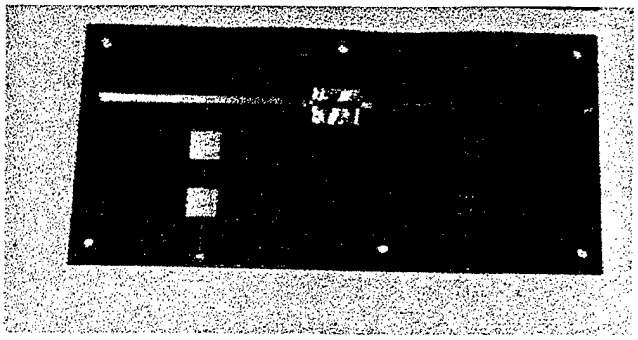

c) Stripline-to-Ground

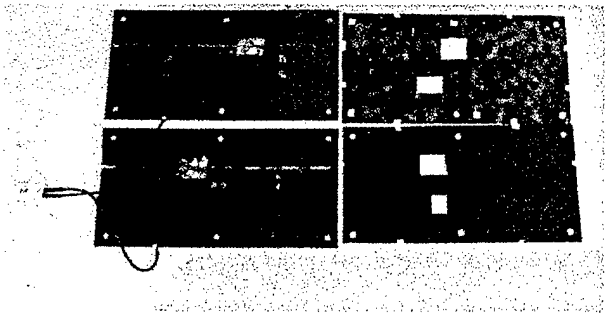

d) Stripline -to-Stripline

FIGURE 4.3-1 TEST CONFIGURATION SAMPLES

5.0 PLASMA, RF ABSORBER OR RF WALL

An interesting observation with regard to plasma is that, from the initially gathered data, it seems the plasma is a RF absorber. If such was the case, then the plasma cannot be used as a phase shifting element. As will be seen, the plasma seemed to act as an RF absorber due to the fact that the stripline was not matched to the electrodes. By inserting tuning stubs near the electrodes on the transmission line, the plasma then reflects most of the energy back to the source.

For plasma to present a wall (an open circuit) to the RF, the electrodes must have a considerable air gap between them. Furthermore, the circuit must be very well tuned using series inductance in conjunction with the capacitance presented by the electrodes. With this combination, the plasma will present an RF wall to the impinging energy.

Figure 5.0-1 shows the single transmission line stripline configuration that yielded very good results, demonstrating the possibility of using plasma as an RF blocking element. The relevant dimensions of the stripline are given below:

$L_l = 0.048"$; $w_l = 0.192"$: $L_s = 0.087"$

$L_e = 0.189"$; $w_e = 0.09"$; $w_{TL} = 0.055"$

The stripline is etched on a duroid substrate with a relative dielectric constant of 2.25 and a thickness of 31mils.

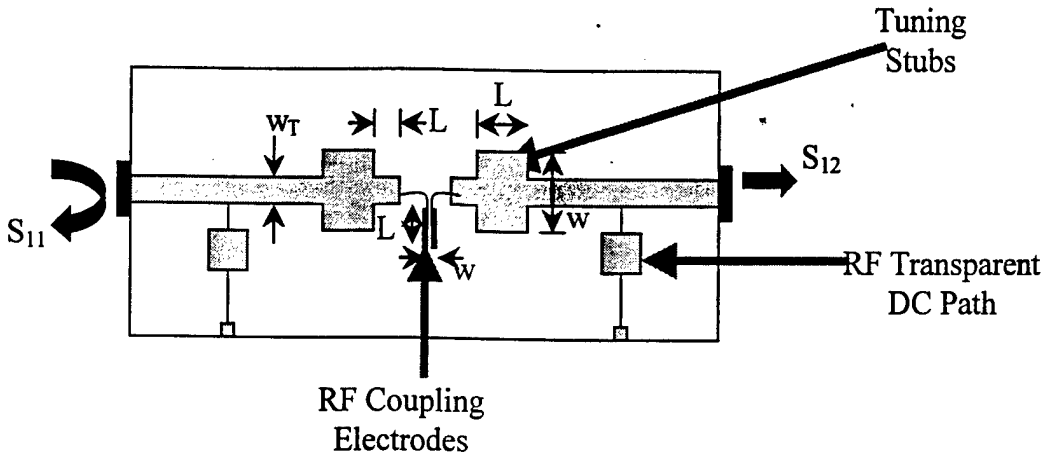

FIGURE 5.0-1 SINGLE TRANSMISSION LINE STRIPLINE

The first set of data shows the reflected and transmitted energy, S_{11} & S_{12} respectively, with and without the presence of plasma (see **Figures 5.0-2** and **Figures 5.0-3**). Figure 5.0-2 presents the data of the stripline without plasma. Notice the passband, 8.75GHz to 9.0GHz, of the stripline seen in the S_{21} measurement (S_{21} & S_{12} are identical measurements since the circuit is symmetrical) and the low level of the reflected energy, S_{11}. In Figure 5.0-3 is presented the reflected and transmitted energy with the presence of plasma (at a NeAr pressure of 15 Torr, with an applied voltage of 350V and a limiting resistor of 20kΩ). Here we conclude, from both measurements, that the plasma within this circuit acts as an RF wall since the reflected RF energy goes from –29.12dB to -1.48dB when the plasma is fired and consequently the transmitted energy (the insertion loss due to the plasma) is attenuated by 10.4dB.

The conclusion then is that plasma can be used within a stripline circuit as a phase shifting element.

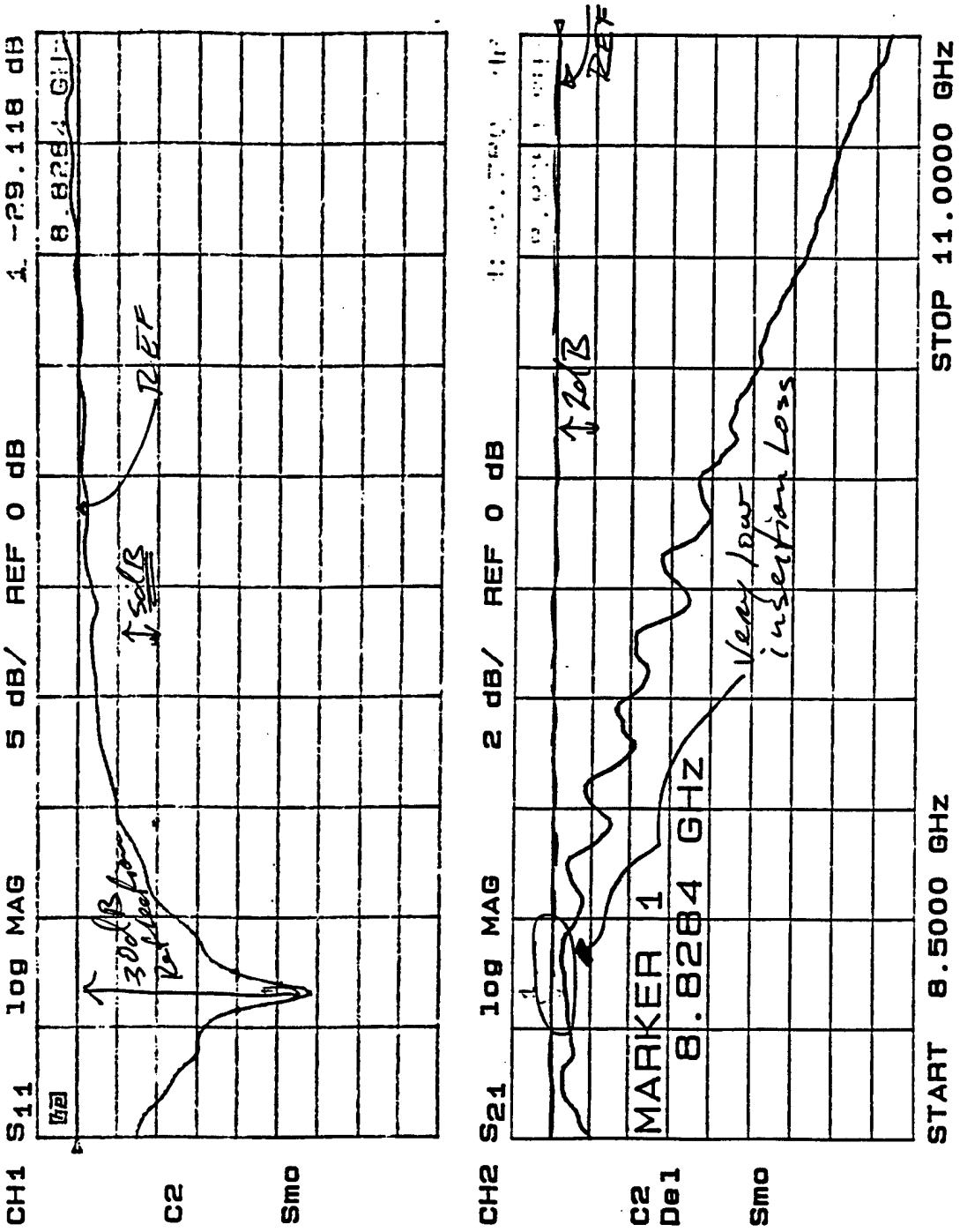

FIGURE 5.0-2 SINGLE TL STRIPLINE SIGNATURE, NO PLASMA

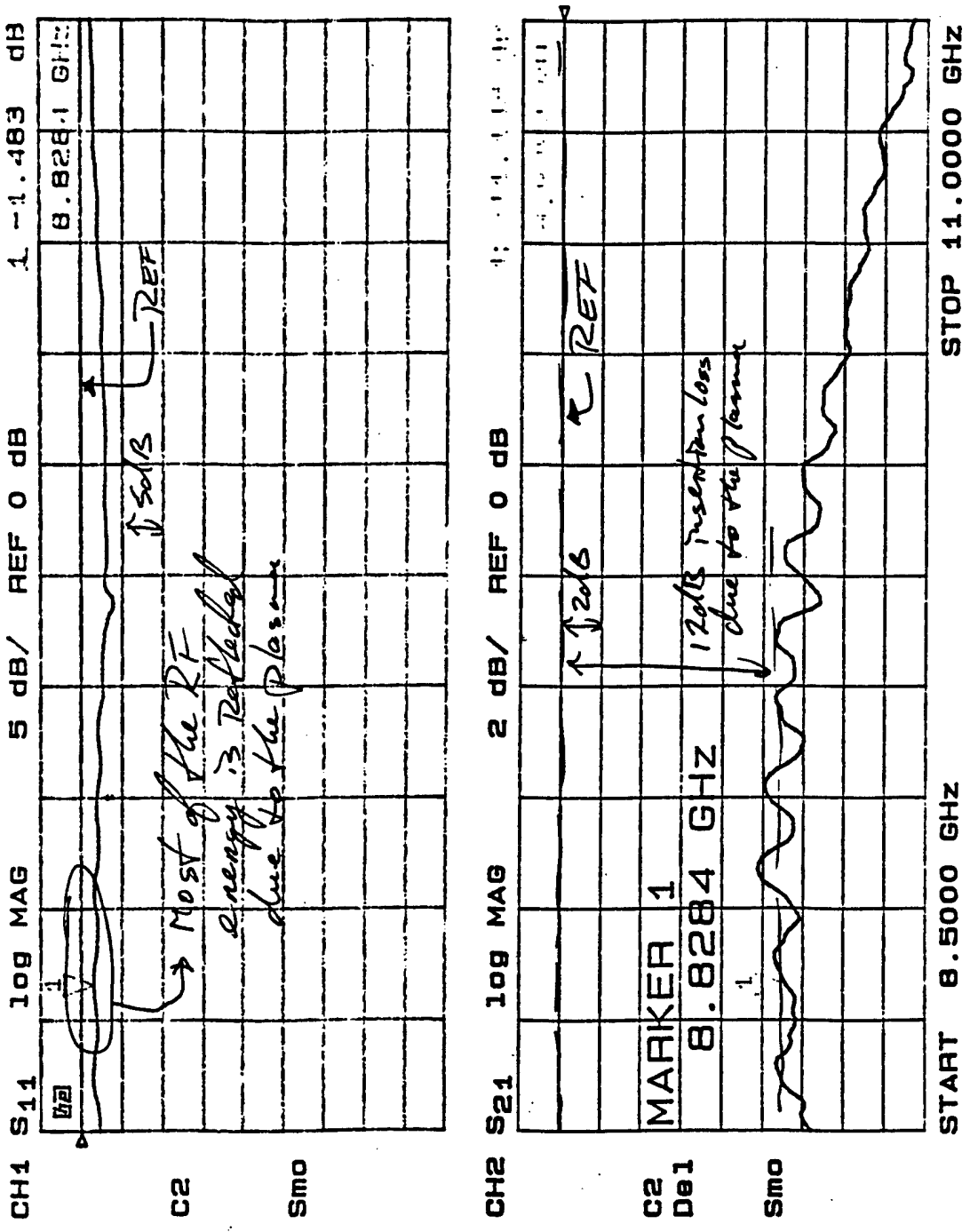

FIGURE 5.0-3 SINGLE TL STRIPLINE SIGNATURE AT 15TORR, 20KΩ & 400VDC

6.0 THE PLASMA PHASE SHIFTER ELEMENT

The plasma phase shifting device consists of two parallel stripline circuits, each segmented by coupling electrodes (where the plasma will fire) and a rat-race (ring hybrid). The reason for using a hybrid is to isolate the input port from the output port. The full system will include a power-distributing element from which the source RF energy will be divided and distributed, with equal phase front, to the phase shifting devices. The energy will then be phase shifted by the plasma stripline circuit before exiting the hybrid where it will be directed toward radiating dipole elements (see **Figure 6.0-1** for a block diagram of the system's RF portion). The hybrid is presented in the next section.

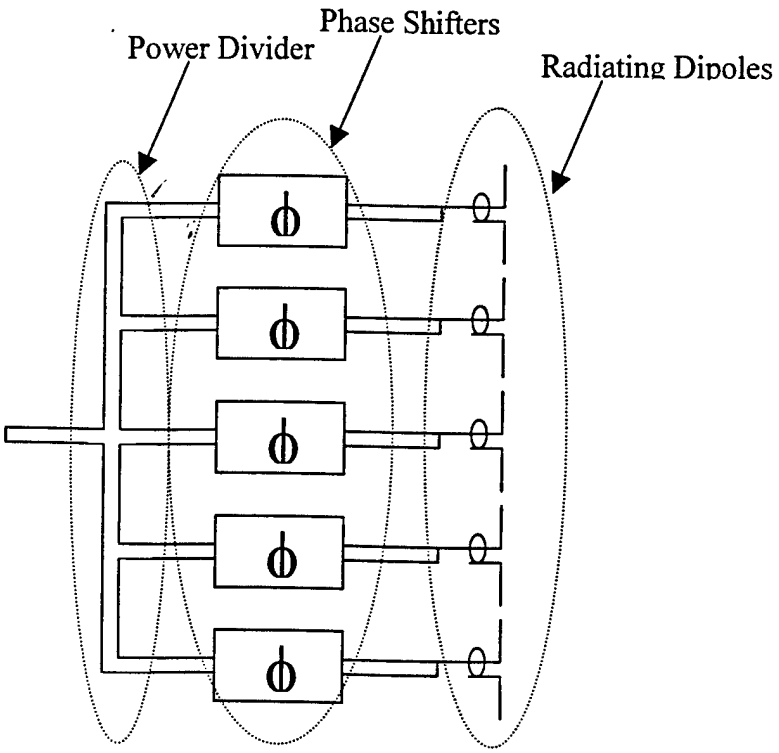

FIGURE 6.0-1 BLOCK DIAGRAM OF THE SYSTEM'S RF PORTION

6.1 THE RAT-RACE

The rat-race, also known as a ring hybrid, is generally used as a power divider. It has high isolation between input & output ports (In & Out shown in **Figure 6.1-1**) and is easily etched on a stripline configuration. The rat-race can be used as an isolation device, a power divider, or in this case a phase shifter.

The rat-race is frequency dependent with an operating bandwidth of approximately 10%. The distance between the ports are as follows (refer **to Figure 6.1-2**):

- Port 1 to Port 3 => $\lambda/4$ (CCW) & $5\lambda/4$ (CW, Clock Wise)
- Port 1 to Port 4 => $3\lambda/4$ (CCW & CW)
- Port 1 to Port 2 => $2\lambda/4$ (CCW) & λ (CW)

A) The rat-race as a power divider:

The input energy, Pin, is equally divided at Port 1, half the power will circulate CW (P_{1A}) and half CCW (P_{1B}). At Port 3 the phase of P_{1A} with respect to P_{1B} is in phase ($\lambda/4$ via CCW and $5\lambda/4$ via CW), therefore the energy adds up and is transferred to Port 3. The same occurs at Port 4; the phase of P_{1A} is coincident with the phase of P_{1B} ($3\lambda/4$ via CCW and $3\lambda/4$ via CW). On the other hand at Port 4 the phases of P_{1A} and P_{1B} are 180° ($\lambda/2$) out of phase. Therefore if Port 3 & 4 are terminated with a matching load, the input energy will be equally distributed to Ports 3 & 4 with minimal energy reflected back to Port 1.

B) The rat-race as a phase shifter:

As stated in the power divider application the rate-race directs half the input energy to Port 3 and half to Port 4. If Ports 3 & 4 are open circuited, such that the energy that goes out of these ports is reflected back to the rat-race, and the transmission line length of Port 4 is 180° ($\lambda/2$) longer than that of Port 3, then

the sum of the input energy is added and directed at Port 2. By including a device in both branches attached to Port 3 & 4, variable phase shifts can be introduced to the input energy.

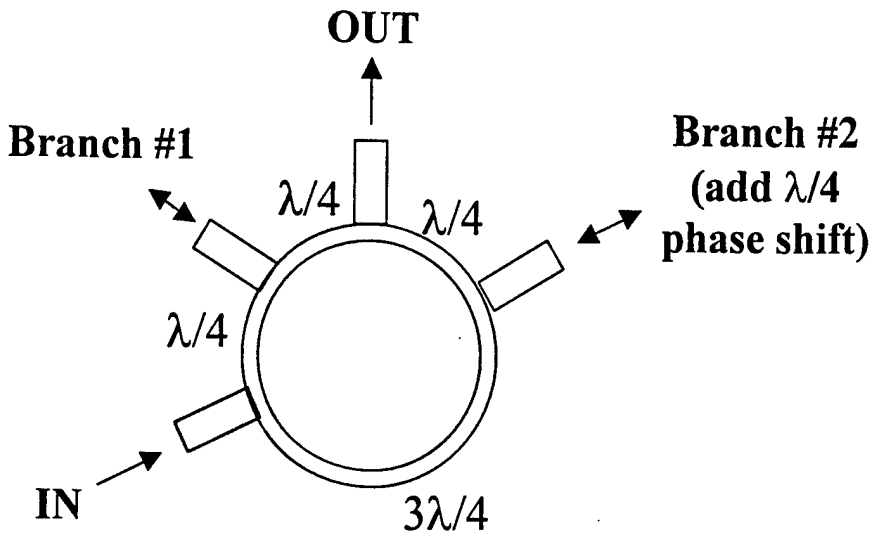

FIGURE 6.1-1 BRANCH LINES OF THE RAT-RACE

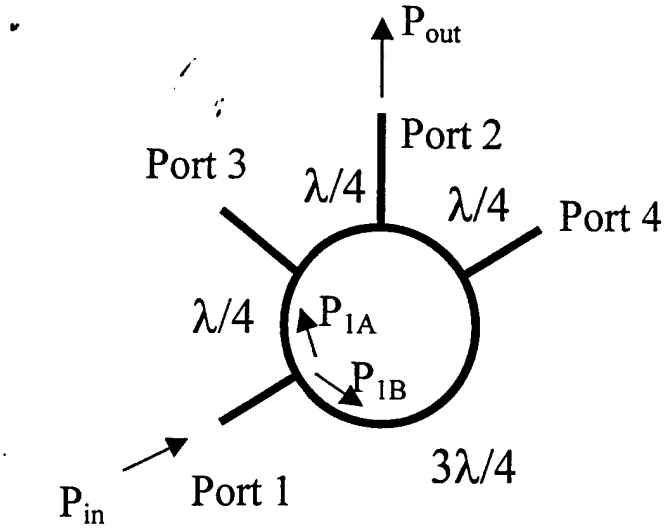

FIGURE 6.1-2 RAT-RACE ROUTING OF INPUT POWER

6.2 THE PLASMA PHASE SHIFTER

This section investigates the basic plasma phase shifting element. In order to reduce the complexity of the system and to properly address the plasma efficiency as a phase shifting element, a commercial hybrid was used instead of the rat-race (ring hybrid). The available commercial hybrid had an operating region between 4GHz and 6GHz; thus a circuit was designed and tuned at the center frequency of 4.7GHz.

The plasma phase shifter test sample consisted of a Narda hybrid connected to the stripline, which is composed of two identical and parallel circuits. The stripline circuits include RF transparent DC path, tuning elements, transmission lines and plasma regions. The actual configuration is shown in **Figure 6.2-1** with the following dimensions:

$L_l = 0.230"$; $w_l = 0.35"$; $L_s = 0.151"$

$L_a = 1.1485"$; $L_b = 2.618"$; $w_{TL} = 0.090"$

The stripline is etched on a duroid substrate with a relative dielectric constant of 2.25. Therefore, at an operating frequency of 4.722 GHz (an available hybrid was chosen for this proof of principle, the one on hand was a Narda with an operating frequency of around 4.5 GHz), the wavelength of the RF energy is:

$$\lambda_\varepsilon = c_0/(f*\mathrm{sqrt}(\varepsilon_r))$$

$$= 3.0E08\mathrm{m/s} / (4.722E09*\mathrm{sqrt}(2.25))$$

$$= 4.235\mathrm{cm} = 1.67"$$

The aim of the analysis is to show that the system can track the phase difference due to the plasma as well as the transmission line length. The length of L_b will be slowly reduced in steps of about $\lambda_\varepsilon/10$, that is around 80 degrees (2*360/10) of phase difference

between steps. In doing so the transmitted power should reflect the phase difference induced by shortening the RF path. If the plasma is in fact a good RF wall, then the phase of the transmitted RF energy should be independent of the TL length L_b.

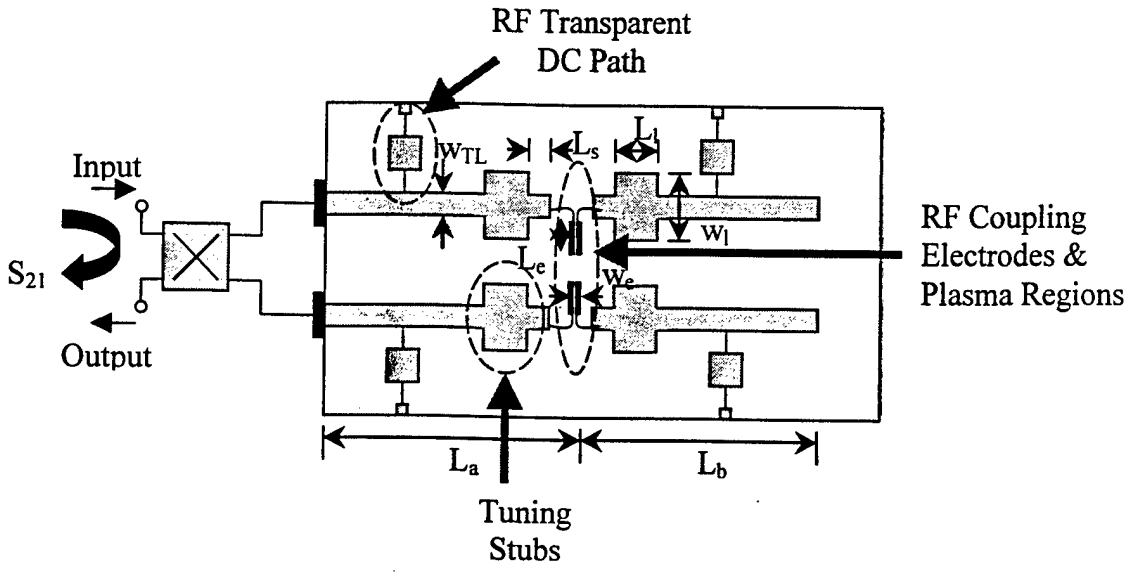

FIGURE 6.2-1 PLASMA PHASE SHIFTER ELEMENT

Figure 6.2-2a shows the magnitude and phase signature of the plasma phase shifter element with L_b equal to 2.618"; S_{21} is the transmitted energy from the input port to the output port of the hybrid referenced to the input level. This is the reference data to which the phase information will be compared. Note the relatively low insertion loss, around 4dB, presented by the plasma phase shifter element (the circuit was grossly tuned).

The circuit was immersed in Neon-Argon (NeAr) gas at a pressure of 14Torrs (ambient pressure is 760Torrs) and DC voltage was applied to the electrodes in the "plasma region" which created the plasma. **Figure 6.2-2b** shows the signature of the

transmitted energy while the plasma is energized. There are two important observations to make here; first, the transmitted power level is practically unaffected by the plasma (which is very good) and secondly, the phase response of the transmitted energy is drastically altered.

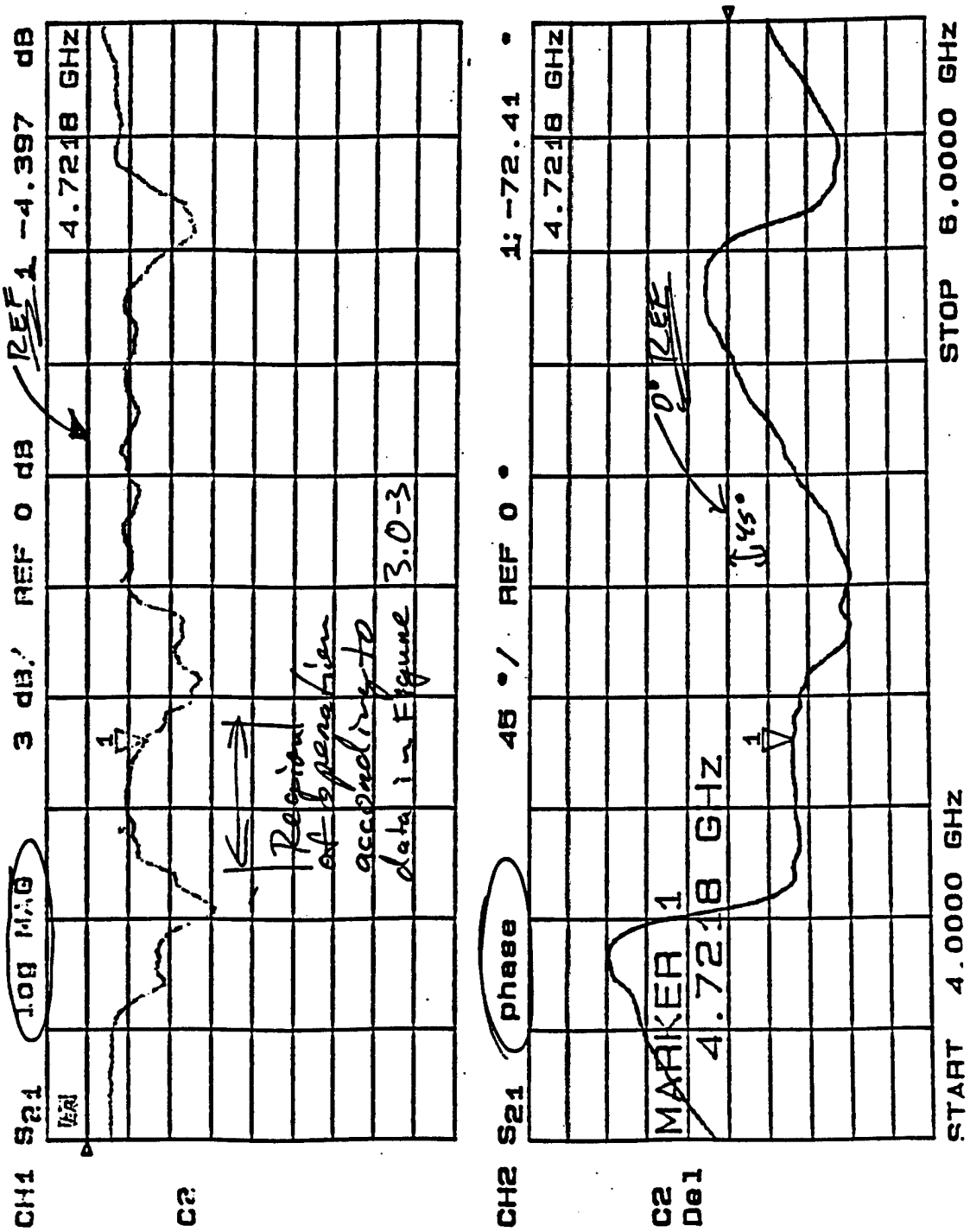

FIGURE 6.2-2A MAGNITUDE & PHASE OF CIRCUIT, L_B = 2.618", NO PLASMA

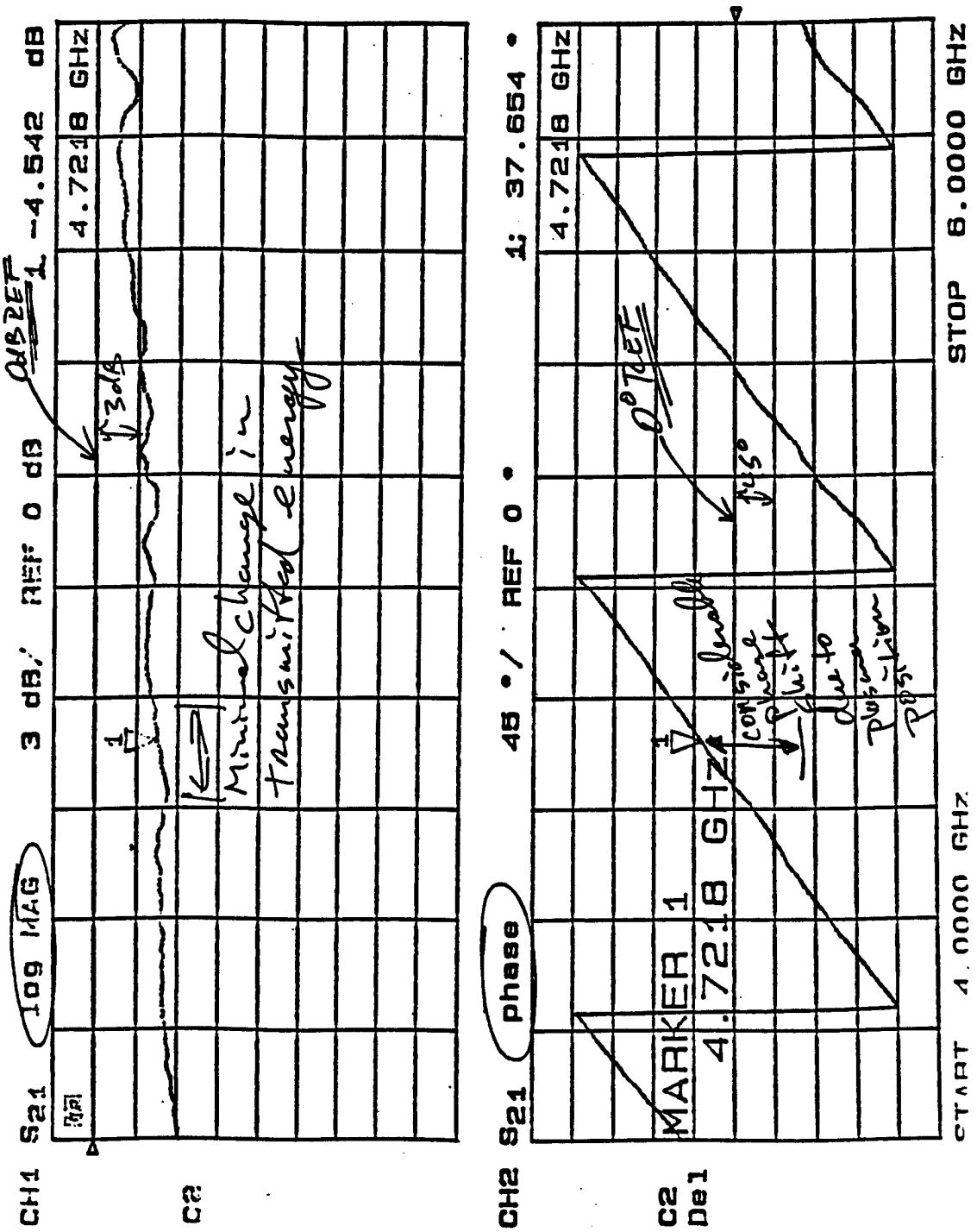

FIGURE 6.2-2B MAGNITUDE & PHASE OF CIRCUIT, L_B = 2.618", 15TORR, 20KΩ, 400VDC

In **Table 6.2-1** is shown the effect of modifying the TL length. As can be seen, the phase difference actually tracks the TL length L_b when the plasma is not energized. Furthermore the phase of the transmitted energy, ϕ_{Plasma}, is in fact independent of the TL length while the plasma is energized. Much data was gathered and normalized to the above baseline data.

TABLE 6.2-1 PLASMA PHASE SHIFTER ELEMENT INVESTIGATION

L_b (inches)	ΔL_b (λ_ε)	$\phi_{NoPlasma}$ (deg.)	ϕ_{Plasma} (deg.)	$\Delta\phi_{Theory}$ (deg.)	$\Delta\phi_{Meas.}$ (deg.)	Plasma Insertion Loss (dB)
2.618	0	–72.41	37.65	0	0	0.15
2.538	0.096	–15.37	51.24	34.6	43.5	0.786
2.478	0.168	15.87	41.51	60.5	82	-0.054
2.437	0.218	51.77	37.68	78	124	0.615
2.358	0.311	93.69	36.75	112	167	-0.058
2.300	0.381	145.25	38.12	137	217	0.168
2.232	0.462	179.22	43.84	167	245	-0.549
2.127	0.588	212.09	46.44	212	275	-1.415

The data is presented in a graphic format in **Figures 6.2-3** through **6.2-5**. In the first graph is plotted the normalized differential phase of the circuit; the phase differential is between the state of plasma OFF and ON. The differential phase is normalized to the phase difference of the longest TL length; that is for L_b equal to 2.618". For example, the measured phase difference for an L_b of 2.618" is 110.06 degrees, which is normalized to 0 degrees, therefore the normalized phase difference for an L_b of 2.538" is 43.45 degrees {that is 110.06 (51.24 - -15.37)}. The theoretical normalized phase difference is calculated as ΔL_b * 360 degrees (ΔL_b is expressed in terms of the wavelength in the dielectric medium). In Figure 6.2-3, note the linearity of the measured normalized phase

difference and also the fact that it follows closely the theory. The important result here is that the measured phase difference is linear and thus any phase shift can be accomplished with the plasma phase shifter element.

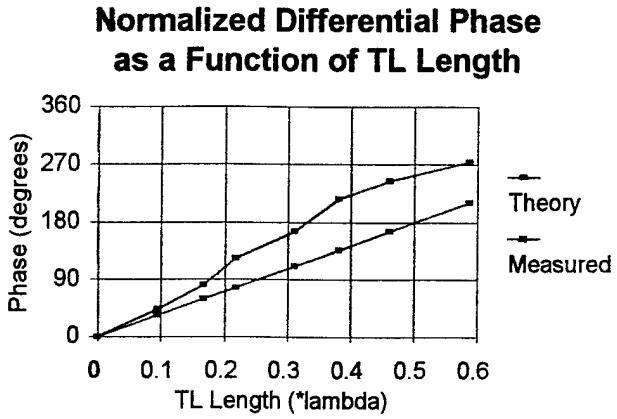

FIGURE 6.2-3 THE NORMALIZED DIFFERENTIAL PHASE

In **Figure 6.2-4** is presented the measured phase of the RF at the output of the plasma phase shifter element, relative to the input phase, as a function ΔL_b. This data shows the efficiency and consistency of the plasma to create an effective RF plasma wall. When the plasma is excited, the output RF phase is effectively constant regardless of the length of the TL beyond the plasma region. Furthermore, without the presence of plasma, the output RF phase displays a constant slope with respect to the TL length.

Another important parameter to consider is the loss presented by the plasma to the transmitted RF energy. Ideally, when the plasma is energized, the level of the transmitted energy should be unaltered, only the phase should change. **Figure 6.2-5** shows the transmitted loss due to the plasma. Notice that the loss oscillated around 0dB, not exceeding 1dB on average. Also, since the electrodes in the plasma region were grossly tuned, the plasma wall actually reflected with better efficiency than in the case without plasma.

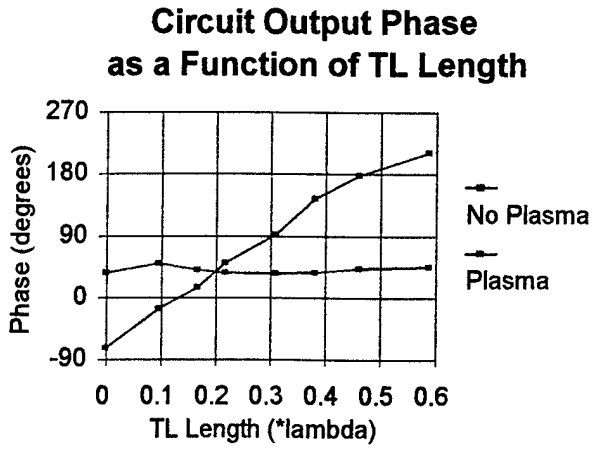

FIGURE 6.2-4 THE PLASMA PHASE SHIFTER ELEMENT OUTPUT PHASE

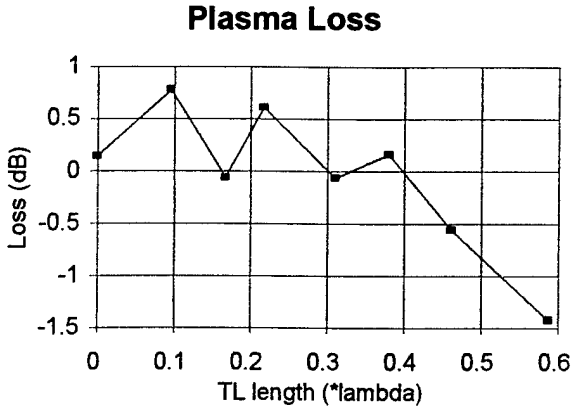

FIGURE 6.2-5 THE PLASMA PHASE SHIFTER ELEMENT INSERTION LOSS

7.0 PLASMA HYSTERESIS

In the previous section the plasma phase shifting element was demonstrated. It was seen that plasma, within a stripline circuit in conjunction with a rat-race, can be used as a phase shifter. Now left to analyze is the plasma hysteresis within the proposed configuration.

7.1 HYSTERESIS IMPORTANCE

The importance of the plasma hysteresis is that it enables a latching configuration thus generating considerable cost savings over conventional phased array systems. The properties presented by the plasma microwave phase shifter are the reason for such savings, these are:

1. The basic device can ultimately be fabricated as a printed circuit, requiring no semiconductor or ferrite components as in current devices. This property alone offers a tremendous savings in array costs.
2. The device, because of the plasma hysteresis, can be configured in a "latching" configuration. That is, the device can be set to a phase state and it will stay at that state until reset. This would be accomplished using a simple holding voltage that would be applied to all plasma elements in the array. In theory (if time permits) a single driver could be used to scan the entire array; the more drivers employed the faster the scan. This is in

contrast to a conventional phase shifter, where a driver is associated with each array element.

3. The device is reciprocal and operates equally well on transmit and receive.

7.1.1 Hysteresis in the Plasma Phase Shifter

The advantages of a plasma phase shifter device over a conventional pin diode device stems from its hysteresis property. The fact that plasma can remain excited with a driving voltage lower than the initial firing voltage allows the complexity of the driving circuitry to be substantially simplified. In a pin diode phased array antenna, the number of drivers required for N by M elements is NxM drivers; that is one driver per pin diode element. Thus for an array of 100 by 100 elements, 10,000 drivers are required. In a plasma phase shifter device individual element settings can be accomplished in a row-column addressing fashion due to the plasma latching capability, see **Figure 7.1.1-1**. (This addressing scheme is used in plasma displays, i.e. computer laptops). Therefore typically N+M drivers are required, that is 200 drivers are required for an array of 100 by 100 elements. This is a substantial reduction in driver requirement over that of a conventional approach by a factor of 50.

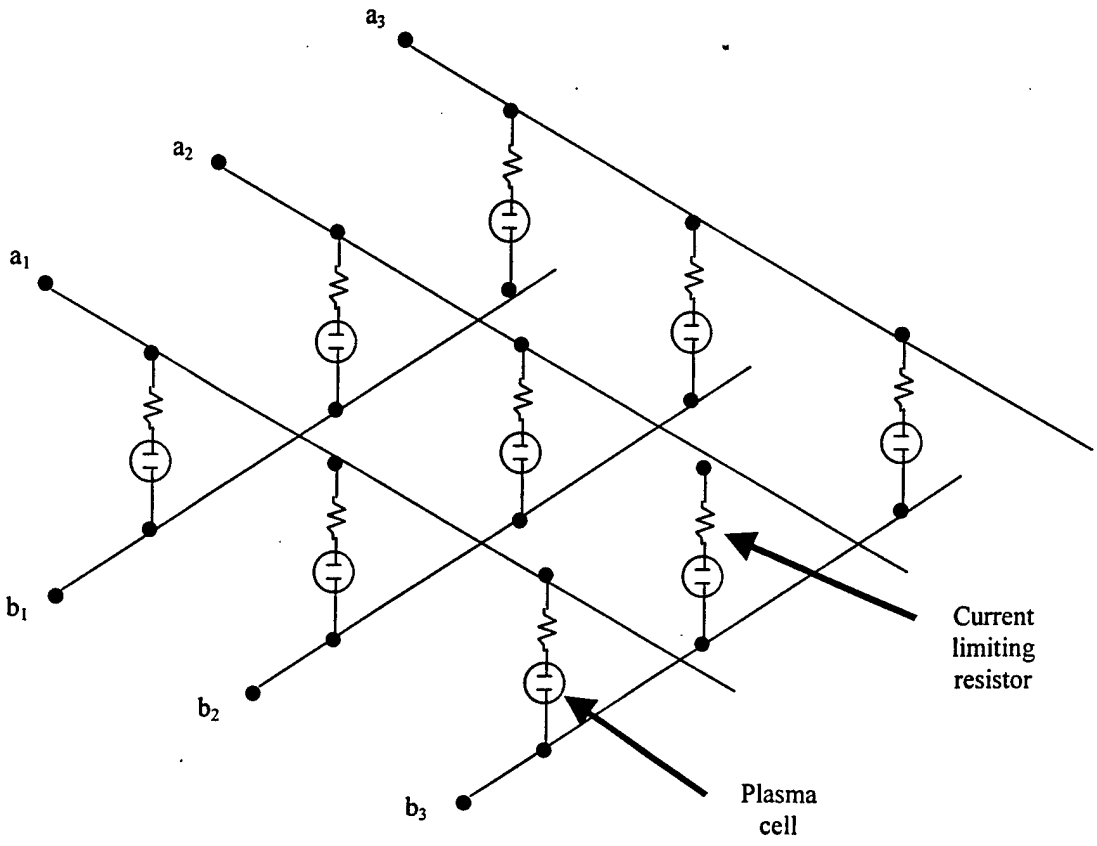

FIGURE 7.1.1-1 ROW-COLUMN ADDRESSING OF THE PLASMA PHASE SHIFTING DEVICE

7.1.2 Plasma Hysteresis Generates Cost Saving

The cost savings of a plasma-scanning array best illustrated by the following example. Consider a two-dimensional phased array scanning antenna operating at 9.3 GHz. The antenna has nominal dimensions of 26 inches by 26 inches. If the array was to scan over a sector of ±45deg. in azimuth and ±45deg. in elevation it would require approximately 1000 radiating elements (N=31 rows by M=31 columns). A phase shifter would feed each element. The following table compares the cost of fabrication using a conventional ferrite phase shifter approach and using the plasma device.

Conventional Ferrite Phased Shifter Approach

Typical ferrite phase shifters at X-band cost around $300/pc for modest volume production. The price is equally divided between the ferrite device and driver.

Cost: Ferrite Phase Shifter Scanning Array

	Each	NxM Number	Total
Ferrite Phase Shifter	$150	1000	$150,000
Drivers	$150	1000	150,000
Support Structure			10,000
Integration & Test			15,000
		Total:	$325,000

Plasma Phase Shifter Element Approach

In the final configuration the phase shifting device would be a simple multilayer printed circuit.

Cost: Plasma Phase Shifter

	Each	Number	Total
Plasma Electrode Printed Circuit		1000 ϕ's	$2,000
Drivers	$150	62 (N+M)	9,300
Support Structure			10,000
Integration & Test			15,000
		Total:	$36,000

As can be seen with this simple example, the cost of the phased array can become relatively inexpensive when compared to the conventional approach. The plasma hysteresis plays an important role in this proposed antenna, without hysteresis, the system cannot be used as a latching device.

7.2 PLASMA HYSTERESIS MEASUREMENTS

7.2.1 Initial Plasma Hysteresis Measurements

The hysteresis phenomenon of the Nixie Tube and of the stripline test sample were measured, as was reported in **MRA P347-05**. The Nixie Tube was used as a baseline for future hysteresis analysis. **Figure 7.2.1-1** plots the plasma drawn current in mA as a function of the applied DC voltage where the arrows depict the direction of the applied voltage (increasing or decreasing). It is seen that the Nixie Tube plasma did not present any hysteresis properties at voltages beyond the plasma turn-on point, 75V. The phenomenon came into action when decreasing the applied voltage below the turn-on point. As the applied voltage decreases, the plasma current slowly diminishes to zero at which point the effective plasma ceases to exist.

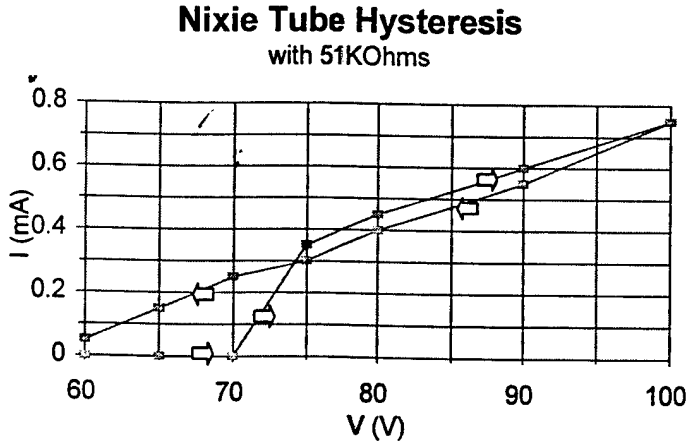

FIGURE 7.2.1-1 NIXIE TUBE PLASMA HYSTERESIS PHENOMENA

The stripline plasma current displayed similar properties as the Nixie Tube plasma current. **Figure 7.2.1-2** plots the plasma current as a function of the applied voltage. As for the plasma in the Nixie Tube, in the stripline configuration it yielded a somewhat

linear relation between the applied voltage and the drawn current beyond the turn-on point. The hysteresis property of the plasma in the stripline was observed when decreasing the applied voltage below the turn-on point (315V) once the plasma has fired.

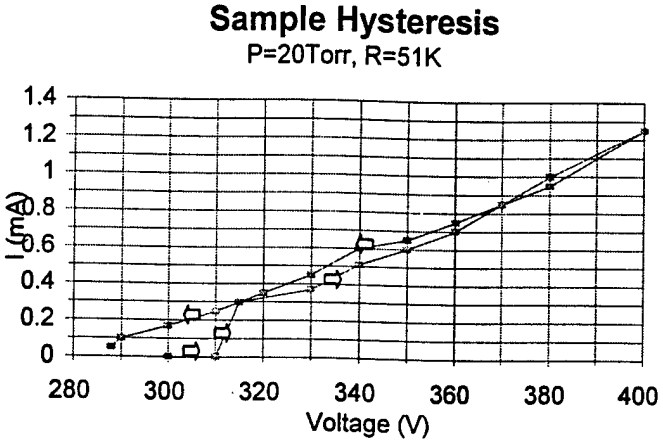

FIGURE 7.2.1-2 STRIPLINE PLASMA HYSTERESIS PHENOMENA

The hysteresis defines a required property of the RF switch, namely that the insertion loss due to the plasma must be in the order of 10 to 20 dB within the hysteresis region. The initial hysteresis measurements proved that plasma does in fact display a hysteresis property. However, the hysteresis curve is not quite the ideal situation. For one thing, the hysteresis span is fairly short (25V) and its starting position coincides with the plasma turn-on voltage position. Further investigation of the hysteresis phenomenon was definitely necessary.

7.2.2 Plasma Hysteresis Research

An extensive literature search was conducted to gather as much information on the hysteresis phenomenon as possible. As it turns out, the gas composition plays an important role in the hysteresis signature of the generated plasma.

In Zhan's paper [1], the authors compare the hysteresis presented by plasma generated in pure hydrogen, H_2, to one generated in a methane-hydrogen, CH_4-H_2, mixture. **Figure 7.2.2-1** shows the hysteresis of plasma in a pure hydrogen gas at a pressure of 300 Pa (approximately 2Torr) and, in **Figure 7.2.2-2**, the hysteresis of plasma in a methane-hydrogen mixture at a neutral gas pressure of 2500Pa (about 20Torr). It was very exciting to see such results since the pure hydrogen results mimic the hysteresis curve that was observed at Malibu Research using a Neon-Argon (NeAr) gas mixture. Other results that confirm the hysteresis signature of plasma in the NeAr gas mixture are the results presented in Merlino's paper [2]. Merlino et al, were the first to talk about the negative deriyative resistance of plasma thus explaining the hysteresis phenomenon of plasma. Furthermore, Merlino presented the hysteresis signature of plasma in a pure Argon gas. Their observations match very well with what was observed in stripline configuration, see **Figure 7.2.2-3**. Notice in Figure 7.2.2-3 the narrow region of hysteresis as well as the fact that hysteresis comes into play at voltages below the plasma turn-on point. Merlino further investigates the hysteresis phenomenon of plasma in pure Argon gas surrounded by a magnetic field strength in another paper [3], see **Figure 7.2.2-4**. Notice here the beautiful plasma hysteresis signature. Unfortunately, it is not feasible to introduce a magnetic field in the stripline configuration.

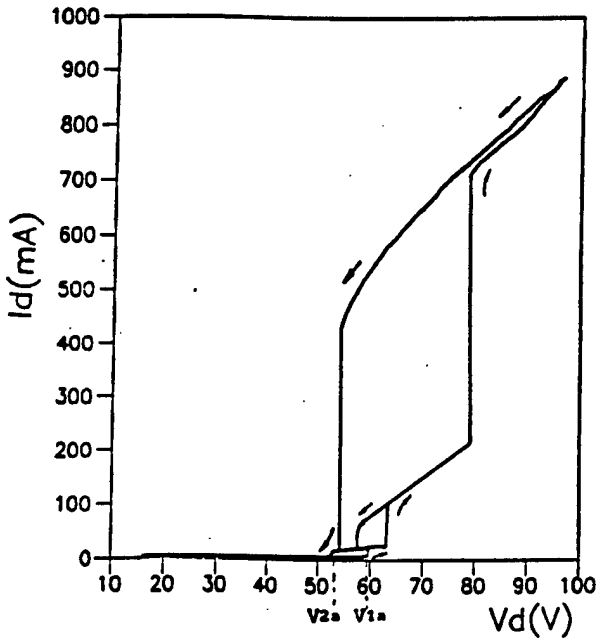

FIGURE 7.2.2-1 ZHAN : PLASMA HYSTERESIS IN PURE HYDROGEN, P= 300 PA

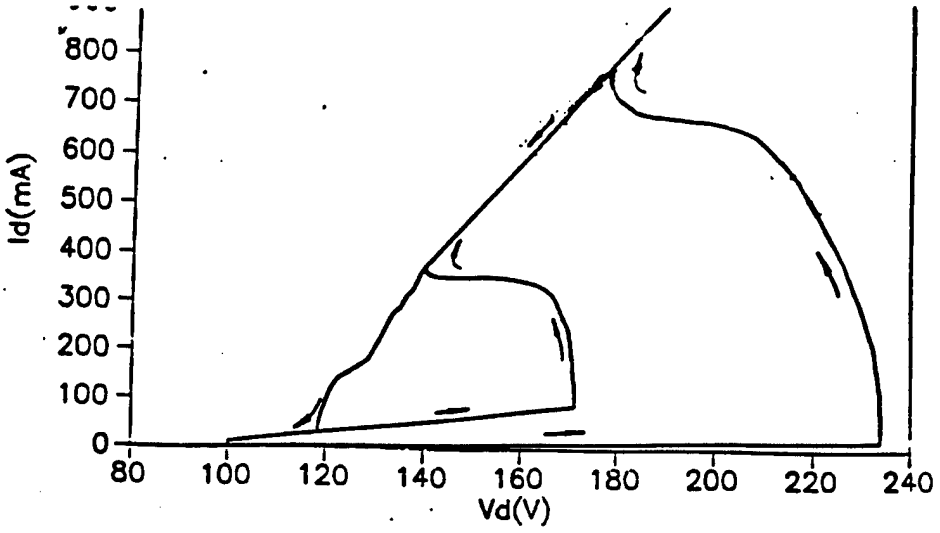

FIGURE 7.2.2-2 ZHAN : PLASMA HYSTERESIS IN CH_4-H_2, P= 2500 PA

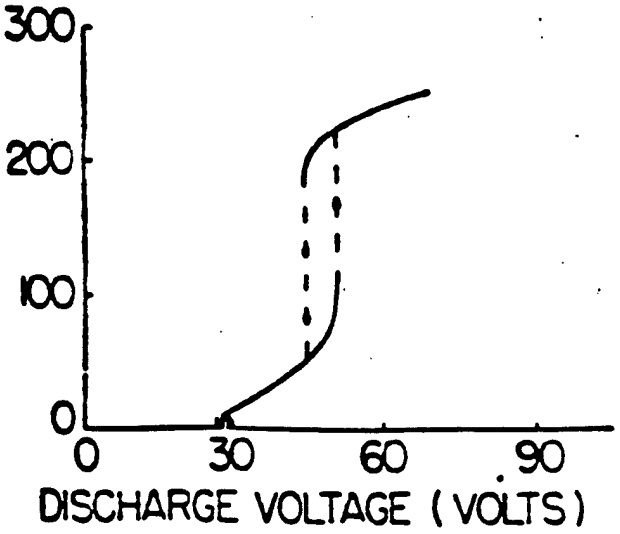

FIGURE 7.2.2-3 MERLINO : PLASMA HYSTERESIS IN PURE ARGON, P= 1MTORR

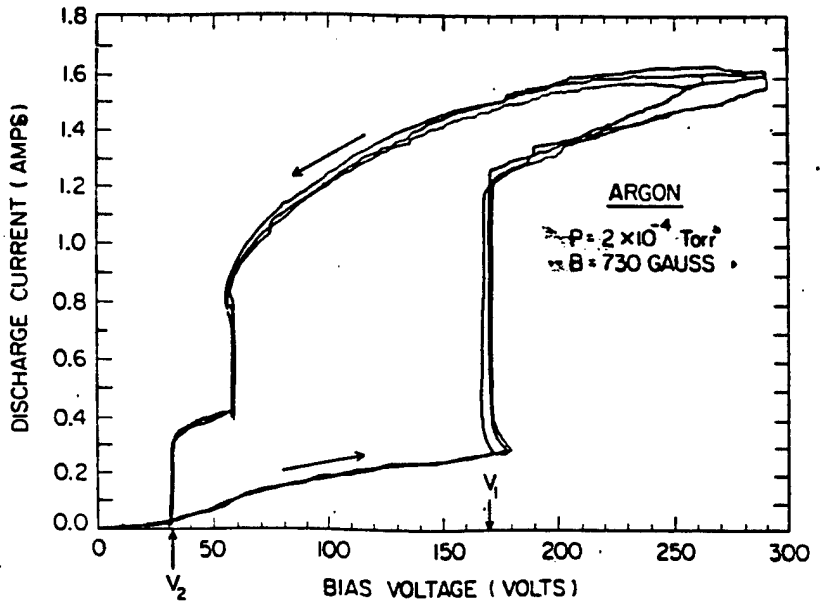

FIGURE 7.2.2-4 MERLINO : PLASMA HYSTERESIS IN PURE ARGON, P= 0.2MTORR, H=730GAUSS

In defining the appropriate gas mixture/purity, the regime under which this application is to work needs to be determined. The regime sought after is the non-collisional regime in which the ions and electrons are relatively free to travel within the plasma with minimal interaction. In the book by Yuri P. Raizer, "Gas Discharge Physics", a few curves are plotted depicting the number of collisions per cm for various gases, see **Figure 7.2.2-5**. As seen in these curves, Helium, He, and Xenon, Xe are two extremes of the different gases shown. Research purity level samples of these two gases were tested.

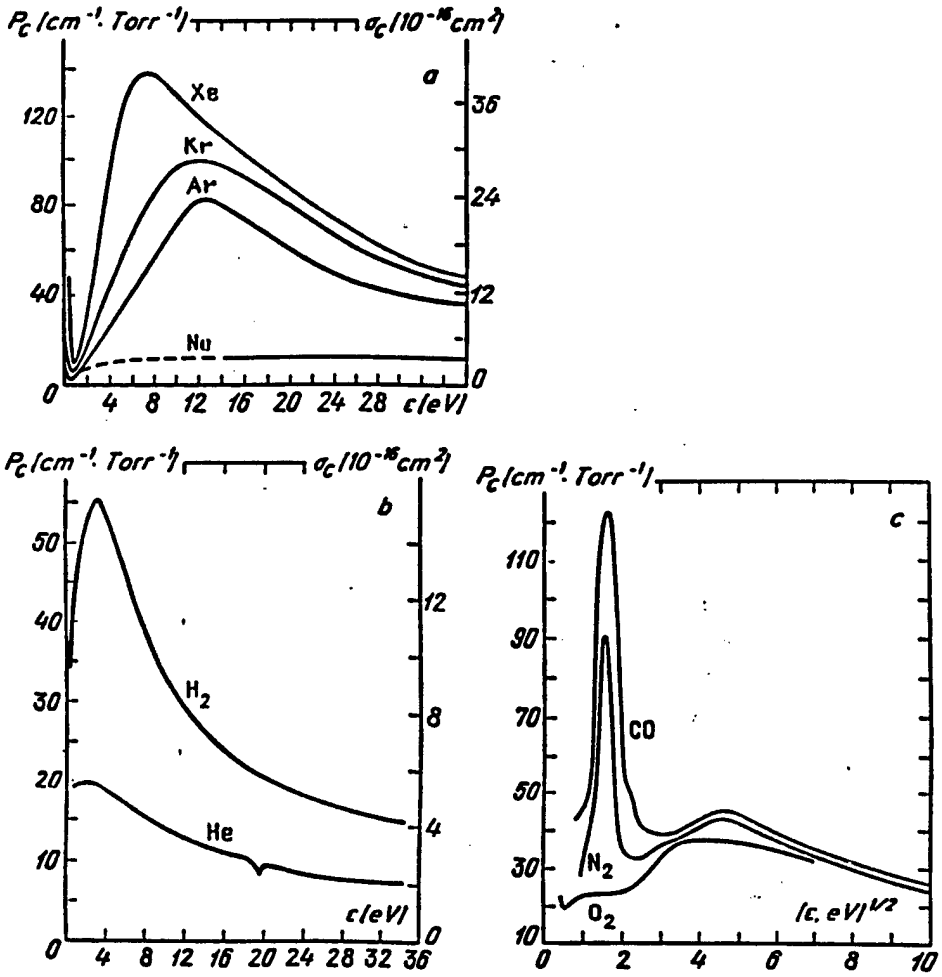

FIGURE 7.2.2-5 PROBABILITIES OF ELECTRON ELASTICCOLLISIONS @ P=1TORR & T=0°C

Also, throughout the literature, many different metals are used for the electrodes. The investigation process consisted of testing various gas mixtures as well as various electrode metal coatings, i.e. Gold, Zinc, Nickel, Rhodium, Silver, Tantalum, as well as Tungsten wires.

7.2.3 Plasma Hysteresis Investigation

7.2.3.1 Hysteresis: Plated Electrodes

The plasma is generated by separating electrons from the molecules/atoms of the gas surrounding the charged anode. Of course, the interaction between the gas and the anode's molecules has a potential to be a major influence in the generation of the plasma and thus, the hysteresis phenomenon of the plasma. The effect of introducing various electrode metals was investigated. The idea was to observe and hopefully determine the best combination of gas-to-electrode combination yielding a near ideal plasma hysteresis response; ideal refers to the plasma phased antenna array application.

Four different metal types of wire plated electrodes were acquired: Gold, Silver, Rhodium and Nickel Sulfurate. The electrodes were inserted in the stripline test circuit as shown in **Figure 7.2.3.1-1**. For this analysis the hysteresis is measured in terms of the current flowing through the plasma region. The plasma current measurement is a good indication of the plasma signature since the RF return loss of the circuit is directly related to the plasma current. The aim was to determine the plasma turn-on voltage and thereafter monitor the hysteresis of the plasma as the voltage is decreased.

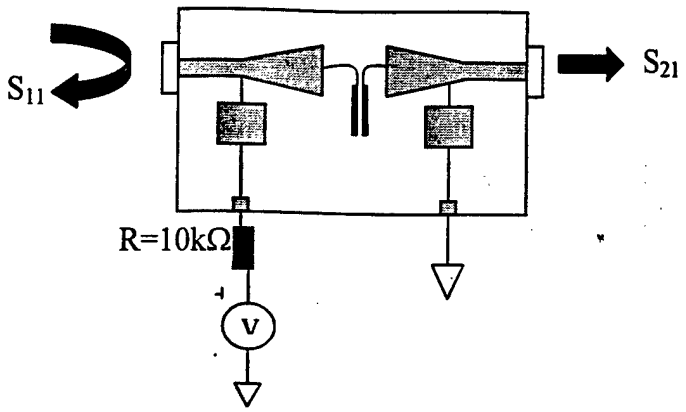

FIGURE 7.2.3.1-1 PLASMA HYSTERESIS MEASUREMENTS IN THE TEST STRIPLINE CIRCUIT

Shown in **Table 7.2.3.1-1** is the result of the data gathered on the various plated electrodes. The Gold plated electrode produced the widest span, between the turn-on and turn-off voltages (170 volts), with a fairly flat current response (60 volts below the turn-on position, the current reduced by only 25%). This result is very encouraging as Gold produced the widest plasma hysteresis span so far encountered. The Silver didn't produce much of a hysteresis (40 volts only) and with minimum induced current (the plasma resistance is fairly high). The Rhodium generated erratic plasma, with non-reproducible phenomenon. Furthermore, the Rhodium required a very high voltage potential to initiate the plasma formation. The Nickel generated a somewhat wide hysteresis (70 Volts), but nothing extraordinary.

Table 7.2.3.1-1 Plated Electrodes Results

Metal	Gold	Silver	Rhodium	Nickel
$V_{turn-on}$ (V)	460	300	490	315
$I(V_{turn-on})$ (mA)	8.3	1.5	9-20	4.6
$I(V_{turn-on}-60V)$ (mA)	6.5	0	NA	1.4
$V_{turn-off}$ (V)	290	260	NA	245

In **Figure 7.2.3.1-2** is shown the plasma hysteresis, in terms of plasma current, for the various metals (excluding the Rhodium for lack of reproducible data). As seen in the previous table and in Figure 7.2.3.1-2, Gold plated electrodes seem to be the best type of electrodes encountered thus far. Unfortunately, the plasma didn't seem to affect the incident RF. The best results were as follows:

- Reflected loss (S11) comes up to a mere –9dB.
- Insertion loss (S21) goes down from –1.08dB to only –5.47dB.

These results are not what one would expect from the measured plasma currents. They are very deceiving when compared to the plasma effect while using the Nixie tube electrodes (see report **MRA P347-05**).

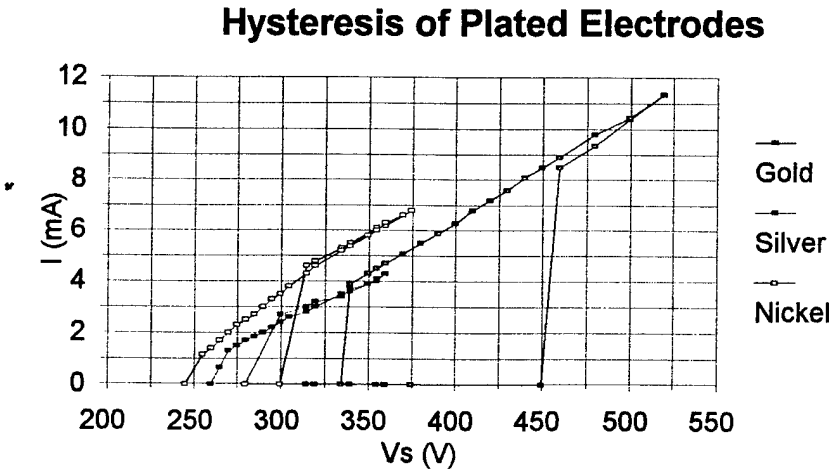

Figure 7.2.3.1-2 Plasma Hysteresis Effect on RF Incident Energy

7.2.3.2 Hysteresis: Gases

Different types of pure gases were tested. First, the hysteresis curve of the NeAr (Neon-Argon) gas is shown in **Figure 7.2.3.2-1**. The NeAr gas has been the preferred gas thus far. The gas pressure was set at 30Torr and a current limiting resistor of 10kΩ was inserted between the DC source and the electrodes. The hysteresis of the Neon-Argon gas is fairly wide and flat; the effective plasma sustain region would be around the 240 volts, 60 volts below the turn-on position.

When the Xenon was fired, nothing much happened in terms of efficient plasma wall, therefore the hysteresis curve in terms of RF was not measured.

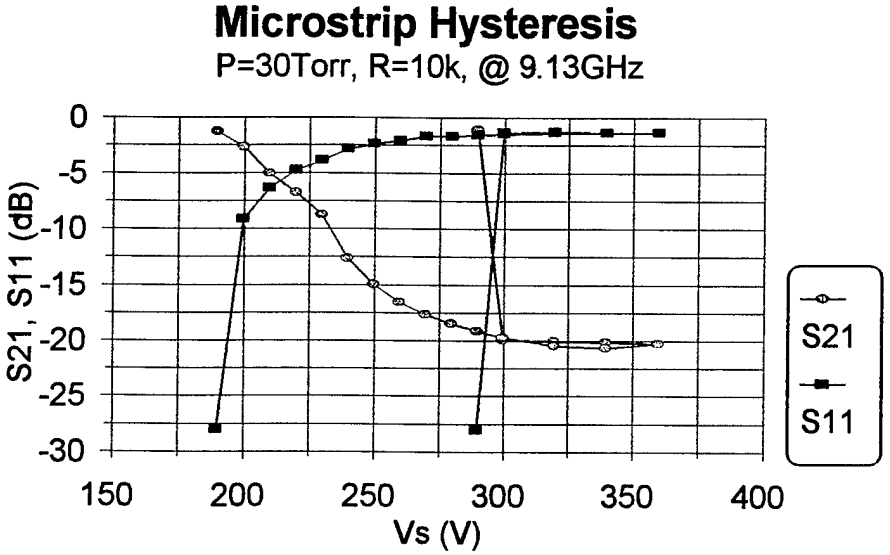

FIGURE 7.2.3.2-1 NE-AR HYSTERESIS SIGNATURE @ P=20TORR & R=10KΩ

The Helium on the other hand produced a very flat and wide hysteresis, see **Figure 7.2.3.2-2**. For Helium to create efficient plasma RF wall, its pressure was set at 60Torr and a 20kΩ current limiting resistor was inserted between the DC source and the

electrodes. The effective plasma sustain region would be around 375 volts; that's 120 volts below the turn-on position! This wider efficient hysteresis span allows for better latching property. Helium was the preferred gas.

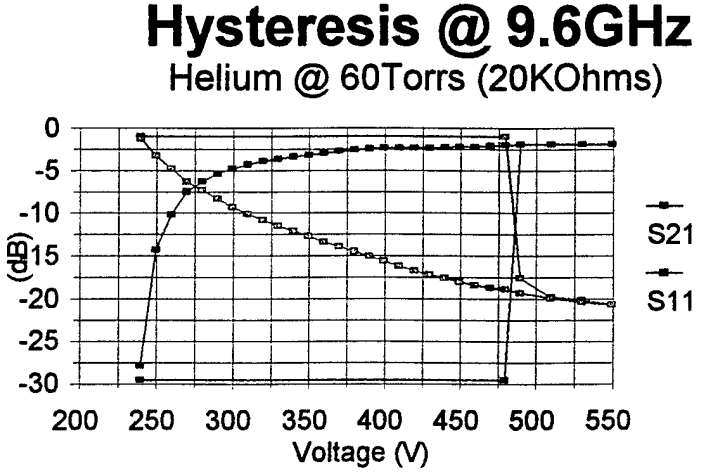

FIGURE 7.2.3.2-2 HELIUM HYSTERESIS SIGNATURE @ P=60TORR & R=20KΩ

8.0 OVERVIEW

This is the final report on the Dynamic FLAPS™ Electronic Antenna, SBIR Phase II. All of the major results and critical considerations were presented. They are summarized in the following:

- Phase I results pointed towards an erroneous conclusion.
- An extensive theoretical investigation revealed that the plasma skin depth, within the proposed application, is not adequate for the plasma display application.
- In the process, an alternate plasma array configuration was defined presenting the same major advantages as the initial proposed design.
- MRA's in-house chamber enabled full control over the plasma parameters in real-time.
- Shown the ability of plasma to create an efficient RF wall.
- Shown the ability of plasma to reflect RF with a consistent phase shift.
- Demonstrated plasma's efficiency in a phase shifting stripline design including the use of hybrids.
- Lack of hysteresis was a major upset that was solved by using a different gas (close to ideal plasma hysteresis signature was obtained using Helium gas).

9.0 REFERENCES

[1] Zhan R. and Jiang X., "Jumps and Hysteresis Effects in CH4-H2 Plasma Discharges", *Journal de Physique III France*, vol. 5, February 1995, 197-202.

[2] Bosh R. and Merlino R., "Sudden Jumps, Hysteresis and Negative Resistance in an Argon Plasma Discharge; I. Discharges with No Magnetic Field", *Contrib. Plasma Phys.*, vol. 26, 1986, 1-12.

[3] Cartier S. and Merlino R., "Observations of Nonlinear Behavior in a Low-Pressure Discharge Column", *IEEE Trans. Plasma Sc.*, PS-12, No. 1, March 1984, 14-18.